MISS SINEAD J LYSTER (Orcid ID : 0000-0002-1188-533X)

Article type : Original Article

Predicting sediment discharges and erosion rates in deep time — examples from the late Cretaceous North American continent

Sinéad J. Lyster[1]*, Alexander C. Whittaker[1], Peter A. Allison[1], Daniel J. Lunt[2] and Alexander Farnsworth[2]

[1]Department of Earth Science and Engineering, Imperial College London, UK.

[2]School of Geographical Sciences and Cabot Institute, University of Bristol, UK.

*s.lyster17@imperial.ac.uk

Acknowledgements

This research was funded by the Natural Environment Research Council (NERC) Science and Solutions for a Changing Planet Doctoral Training Partnership (DTP). DJL and AF acknowledge support from NERC grant NE/K014757/1, Cretaceous-Paleocene-Eocene: Exploring Climate and Climate Sensitivity. We thank Getech Group Plc. for providing palaeo-digital elevation models (palaeoDEMs) used in this study and for useful discussions (particularly Andrew Quallington, Meg Galsworthy and Peter Webb). We would also like to thank Stephen Watkins (University of Geneva), Alfio Alessandro Chiarenza (Perot Museum of Nature and Science) and Lewis Jones (Imperial College London) for helpful discussions and support relating to data sets and methodology. Finally, we would like to thank the three reviewers, John Holbrook, Janok Bhattacharya, and one anonymous reviewer, whose detailed feedback and useful suggestions have improved this paper.

Abstract

Depositional stratigraphy represents the only physical archive of palaeo-sediment routing and this limits analysis of ancient source-to-sink systems in both space and time. Here we use palaeo-digital elevation

models (palaeoDEMs; based on high-resolution palaeogeographic reconstructions), HadCM3L general circulation model (GCM) climate data and the BQART suspended sediment discharge model to demonstrate a predictive, forward approach to palaeo-sediment routing system analysis. To exemplify our approach, we use palaeoDEMs and HadCM3L data to predict the configurations, geometries and climates of large continental catchments in the Cenomanian and Turonian North American continent. Then, we use BQART to estimate suspended sediment discharges and catchment-averaged erosion rates and we map their spatial distributions. We validate our estimates with published geologic constraints from the Cenomanian Dunvegan Formation, Alberta, Canada, and the Turonian Ferron Sandstone, Utah, USA, and find that estimates are consistent or within a factor of two to three. We then evaluate the univariate and multivariate sensitivity of our estimates to a range of uncertainty margins on palaeogeographic and palaeoclimatic boundary conditions; large uncertainty margins (≤50%/±5°C) still recover estimates of suspended sediment discharge within an order of magnitude of published constraints. PalaeoDEMs are therefore suitable as a first-order investigative tool in palaeo-sediment routing system analysis and are particularly useful where stratigraphic records are incomplete. We highlight the potential of this approach to predict the global spatio-temporal response of suspended sediment discharges and catchment-averaged erosion rates to long-period tectonic and climatic forcing in the geologic past.

Keywords

Sediment discharges, Source-to-sink, North America, Late Cretaceous, Palaeogeographies, General circulation models

1. Introduction

1.1 Study rationale

Erosion and sediment discharge is an intrinsic part of the Earth surface system, with impacts on climate (Molnar & England, 1990), biogeochemical fluxes (Beusen et al., 2009; Bernard et al., 2011; Dürr et al., 2011) and long-term carbon cycling (Blair et al., 2004; Leithold et al., 2016), as well as feedbacks between tectonics and topography at Earth's surface (Willett, 1999; Wobus et al., 2006; Allen, 2008a, 2008b). As such, reconstruction of sediment routing and sediment discharges is essential to understanding the coupling of climate, tectonics and surface processes over geological timescales (Whipple & Meade, 2006; Allen, 2008a; Whipple, 2009; Whittaker, 2012).

Depositional stratigraphy represents the time-integrated product of mass transfer across Earth's surface via palaeo-sediment routing systems (Allen, 2008a; Romans & Graham, 2013; Romans et al., 2016). In

principle, it can be used to decipher catchment, erosion and sediment discharge characteristics (Allen et al., 2013; Holbrook & Wanas, 2014; Michael et al., 2014), as well as tectonic and climatic events in the geologic past (Duller et al., 2010; Armitage et al., 2011; Whittaker et al., 2011). However, palaeo-sediment routing system analysis is typically limited by the incomplete or absent geologic record of terrestrial catchments (Sadler, 1981; Romans & Graham, 2013; Romans et al., 2016).

Techniques to quantitatively constrain sediment discharges and erosion rates in deep time include use of time-constrained sediment thicknesses/volumes (Walford et al., 2005; Galloway et al., 2011; Hampson et al., 2014), channel-fill palaeohydrology (Holbrook & Wanas, 2014; Lin & Bhattacharya, 2017; Sharma et al., 2017), grain-size sequestration trends (Duller et al., 2010; Whittaker et al., 2011; Michael et al., 2014) and reconstructed palaeocatchment characteristics (Sømme et al., 2009; Allen et al., 2013). This latter approach also includes the application of empirical sediment discharge models to ancient systems (Allen et al., 2013; Lin & Bhattacharya, 2017; Zhang et al., 2018). Additional approaches include techniques to constrain denudation rates using apatite fission track (AFT) ages (Tinker et al., 2008; Vernon et al., 2008; Cederbom et al., 2011; Painter et al., 2014) and large-scale fluvial inversion models based on present-day river long profiles (Paul et al., 2014; Stephenson et al., 2014). These methods are all useful but are subject to caveats associated with methodological assumptions, errors and uncertainties of measurement tools, and the restricted spatial and temporal resolution of data. Consequently, investigating sediment routing at continental and global scales in the geologic past remains a pre-eminent research challenge.

In this study we evaluate high-resolution palaeogeographies as a first-order investigative tool in palaeo-sediment routing system analysis. Palaeogeographic reconstructions offer a conceptual model of Earth's topography during time-integrated 'slices' of the geologic past (Markwick & Valdes, 2004; Markwick, 2018) and improvements to reconstruction methods and data sets over recent decades (see review in Markwick (2018)) have significantly enhanced our understanding of palaeotopography. Digitisation of these models as palaeo-digital elevation models (palaeoDEMs) is now employed by various research communities (e.g. Bonne, 2014; Lunt et al., 2016; Chiarenza et al., 2019) and routine application of palaeoDEMs to palaeoclimate modelling experiments (tested and calibrated against proxy records) suggests robustness at coarse resolution (Hunter et al., 2008; Tindall et al., 2010; Craggs et al., 2012; Tabor et al., 2016). Coupling of palaeoDEMs with palaeoclimate data therefore offers novel opportunities to explore Earth surface processes in the geologic past.

Here, we (1) use palaeoDEMs to reconstruct large continental palaeocatchments in North America during the Cenomanian and Turonian stages of the late Cretaceous; (2) predict suspended sediment discharges and erosion rates using data from HadCM3L, a coupled atmosphere–ocean general circulation model

(GCM), and the BQART sediment discharge model (Syvitski & Milliman, 2007); (3) compare estimates of suspended sediment discharges with predictions derived from previous field-based approaches; and (4) test the univariate and multivariate sensitivity of our approach. Our results provide insights to the utility (and fidelity) of palaeogeographic reconstructions within a predictive, forward approach to palaeo-sediment routing system analysis. Further, sensitivity analysis defines the limits and applications of our approach. We deliver first-order estimates of palaeodrainage networks, suspended sediment discharges and erosion rates in the Cenomanian and Turonian North American continent, which coincide with the Cretaceous Thermal Maximum.

1.2 Research background

i. Reconstructing sediment discharges in ancient source-to-sink systems

Techniques to reconstruct sediment discharges in the geologic past have generally focused on the thickness, volume and characteristics of time-constrained depositional stratigraphy to estimate, or back-calculate, onshore sediment discharges (e.g. Walford et al., 2005; Galloway et al., 2011; Hampson et al., 2014). For example, Galloway et al. (2011) constrained sediment discharges to the Gulf of Mexico during the Cenozoic, which have since been corroborated by independent approaches (e.g. Petter et al., 2013; Zhang et al., 2018). A closed system is often assumed, but efforts have been made to account for along-strike sediment transport where the source-to-sink system is not fully closed (e.g. Hampson et al., 2014).

Alternatively, Holbrook and Wanas (2014) demonstrated use of channel palaeohydrology in fluvial stratigraphy to estimate sediment discharges in ancient source-to-sink systems of the Cenomanian Bahariya Formation, Egypt. This approach has also been used to understand sediment routing in late Cretaceous North America (Lin & Bhattacharya, 2017; Sharma et al., 2017), which we explore later in this study. While this method does not require a closed system, it assumes that, for a given time interval, the total sediment volume passing through a cross section of the trunk channel is equal to the sediment volume contributed by the source area and the sediment volume deposited in the sink region (Holbrook & Wanas, 2014). This method therefore requires preservation of a trunk channel significantly inland of the palaeoshoreline.

Measures of sediment calibre can be used to calculate grain-size fining rates, which are dependent on the distribution of tectonic subsidence (Whittaker et al., 2010) and sediment discharge (Fedele & Paola, 2007; Duller et al., 2010; Whittaker et al., 2011). While quantitative inversion of grain-size fining trends in fluvial stratigraphy can successfully recover spatio-temporal variations in sediment discharge and tectonic

subsidence (Duller et al., 2010; Whittaker et al., 2011), this approach requires significant preservation of the sediment routing system in space and time.

Ultimately, all stratigraphic methods are limited by the need for well-preserved and age-constrained outcrop/subsurface data that ideally represent a closed or partially-closed system. Stratigraphic methods (particularly field-based methods) are also inherently time consuming and often recover estimates that are precise to only one order of magnitude.

An alternative, catchment-based, strategy is to forward model sediment discharges using the geometries and characteristics of ancient terrestrial catchments. Allen et al. (2013) made first-order estimates of sediment discharges from Paleogene palaeocatchments in the Pyrenees, Spain, by reconstructing catchment characteristics from field observations and applying a bulk diffusive model. In their model, sediment discharge is the product of an incising drainage network, where bulk diffusivity is controlled by mean annual precipitation and the length over which precipitation is concentrated. However, this model (as well as others) requires long term erosional parameters to be deduced *a priori*. Alternatively, catchment-based forward estimates of sediment discharge can also be made by relatively simple sediment discharge models such as BQART (Syvitski & Milliman, 2007). BQART is an empirically-derived multiple regression model of long-term (>30 years) average suspended sediment load. Mean annual suspended sediment load, *Qs*, can be approximated by

$$Q_s = \omega \mathrm{B} \mathrm{Q}^{0.31} \mathrm{A}^{0.5} \mathrm{R} \mathrm{T} \text{ for } \mathrm{T} \geq 2°\mathrm{C}, \quad (1a)$$

$$Q_s = 2\omega \mathrm{B} \mathrm{Q}^{0.31} \mathrm{A}^{0.5} \mathrm{R} \text{ for } \mathrm{T} < 2°\mathrm{C}, \quad (1b)$$

where *Qs* is in units of MT/yr (1 MT = 10^9 kg), ω is a unit conversion constant of 0.0006, Q is water discharge (km^3/yr), A is drainage area (km^2), R is maximum relief (km), and T is mean annual temperature (°C). B is a glacial, lithologic and anthropogenic factor (see Syvitski and Milliman (2007)). Syvitski and Milliman (2007) tested BQART on a global database of 488 rivers that drain 63% of Earth's surface and showed that BQART accounts for 96% of variance in observed *Qs*. When B is set to 1, Syvitski and Milliman (2007) showed that BQART explains 66% of variance in observed *Qs*, and that estimates of *Qs* are calculated within one order of magnitude, and most within a factor of five, of observed *Qs*.

Relative to other suspended sediment discharge models (e.g. Pelletier, 2012; Cohen et al., 2013), BQART is well-suited to geologic application as it has comparatively low data requirements (see discussion in Allen et al., 2013; Helland-Hansen et al., 2016; Eide et al., 2018) — this is ideal when one is dealing with an incomplete rock record as it minimises assumptions. Various authors have used BQART to model *Qs* in

Quaternary systems on 10^2–10^5 yr timescales, and have calibrated BQART estimates with preserved sediment thicknesses (Sømme et al., 2011; Watkins et al., 2018) or catchment-averaged denudation rates derived from cosmogenic ^{10}Be (Hidy et al., 2014). In particular, BQART has been used to investigate temporal variation in *Qs* across glacial–interglacial periods (Garvin, 2008; Hidy et al., 2014; Watkins et al., 2018). To date, translation of BQART to ancient systems on 10^6–10^8 yr timescales includes comparison of BQART with *Qs* estimates derived from alternative methods (Allen et al., 2013; Lin & Bhattacharya, 2017), use of BQART where regional palaeogeography is well-understood (Zhang et al., 2018), and inverse applications, where constraints and/or estimates of *Qs* from depositional stratigraphy have been used to predict palaeotopography (e.g. Carvajal & Steel, 2012; Sømme et al., 2013).

Application of BQART to ancient systems is infrequent as it requires constraints on palaeocatchment drainage area, maximum relief, temperature and water discharge; deducing these parameters from depositional stratigraphy at continental scales is not usually possible as the geologic record of terrestrial catchments is incomplete (and erosional source regions are inherently not preserved). In this study we translate BQART to ancient systems on continental scales; to achieve this we require robust palaeogeographies, to characterise palaeodrainage, and robust palaeoclimate estimates.

ii. Palaeogeographies and HadCM3L

Access to palaeoDEMs and palaeoclimate modelling results offers new opportunities to constrain BQART input parameters, especially on large spatio-temporal scales. Coupling of these novel data sets enables us to reconstruct catchment geometries and catchment-averaged palaeoclimates; with BQART we can then model both *Qs* and catchment-averaged erosion rates on a variety of spatial and temporal scales.

Palaeogeographic reconstructions are of increasing scientific importance across fields such as pre-Quaternary palaeoclimate modelling and hydrocarbon exploration (evaluation of play element distributions, e.g. Markwick (2018)). Major advances to the resolution of palaeogeographies are attributed to growth of the extensive lithologic, tectonic and palaeontologic data sets that underpin them (see discussion in Markwick & Valdes, 2004; Markwick, 2018). Markwick and Valdes (2004) developed a method that uses geographic information systems (GIS) to digitise high-resolution palaeogeographies as palaeoDEMs and facilitate their use in palaeoclimate modelling, lithofacies retrodiction and source-to-sink analysis. These palaeoDEMs can subsequently be used as palaeogeographic boundary conditions in GCMs such as HadCM3L (e.g. Lunt et al., 2016).

HadCM3L is a coupled atmosphere–ocean GCM that was developed at the Hadley Centre for Climate Prediction and Research at the UK Meteorological Office; it comprises linked atmosphere, ocean,

vegetation and sea-ice models and is one of the earliest GCMs to prevent climate drift without requirement of flux adjustments (Gordon et al., 2000; Pope et al., 2000). Relative to more recent and/or higher resolution GCMs, HadCM3L is fast and allows millennial and multi-millennial-scale integrations (Farnsworth et al., 2019), which is essential for deep-time modelling work where the initial condition may be far from the final equilibrium state — HadCM3L has been used in numerous pre-Quaternary palaeoclimate studies (Lunt et al., 2007; Tindall et al., 2010; Craggs et al., 2012; Lunt et al., 2016).

2. Study area

We focus on the Cenomanian and Turonian North American continent, where published estimates of *Qs* offer opportunities to validate our palaeoDEM–HadCM3L–BQART approach. Key tectono-geographic features of this region include the Sevier orogenic fold-and-thrust belt and its adjacent foreland basin, the Western Interior Basin (WIB; Figure 1) (Armstrong, 1968; Jordan, 1981; Cross, 1986; DeCelles, 1994). The WIB formed from eastward subduction of the Farallon plate beneath the western margin of North America, which generated relatively uniform, long-wavelength dynamic subsidence across the continent (Liu et al., 2011; Liu et al., 2014). Superimposed on this was a narrow 120–180 km region of more pronounced subsidence in the Sevier fold-and-thrust belt foredeep, driven by east–west crustal shortening and short-wavelength flexural loading (Kauffman, 1977; Pang & Nummedal, 1995; Liu & Nummedal, 2004). This led to flooding of the continent during the middle and late Cretaceous by the Western Interior Seaway (WIS) (Figure 1), a north–south trending epicontinental seaway that connected polar oceans in Arctic Canada with subtropical oceans in the Gulf of Mexico (Kauffman, 1977; Hay et al., 1993; Kauffman & Caldwell, 1993; Miall et al., 2008).

The palaeogeographic evolution of the Cretaceous North American continent is well-understood and has been comprehensively reviewed (Kauffman & Caldwell, 1993; Roberts & Kirschbaum, 1995; Hay et al., 1999; Miall et al., 2008), especially in the context of palaeodrainage evolution (Bhattacharya et al., 2016). This has largely been constrained by depositional stratigraphy and detrital zircon (DZ) geochronology, at both regional (Szwarc et al., 2015; Bartschi et al., 2018; Pettit et al., 2019) and continental scales (Roberts & Kirschbaum, 1995; Benyon et al., 2014; Blum & Pecha, 2014; Finzel, 2014). Clastic sediment input from the western WIS margin dominated the WIB and, at lowstand, rivers coalesced to form major fluvial drainage networks (Miall et al., 2008; Bhattacharya et al., 2016). Whereas, the eastern WIS margin was bounded by lowlands on the stable North American craton; sediment input here was comparatively limited and resulted in accumulation of thin stratal sequences (Witzke et al., 1983; Hay et al., 1993; Witzke & Ludvigson, 1994; Brenner et al., 2003; Miall et al., 2008). On this eastern margin, transcontinental fluvial systems transported Appalachian-derived sediment west to the WIB back-bulge

and also to the north (Finzel, 2014). The Appalachian–Ouachita cordillera formed a continental drainage divide that separated these systems from drainage to the Atlantic Ocean, Gulf of Mexico (GoM) and the southeasternmost WIS margin (e.g. Adams & Carr, 2010; Blum et al., 2017).

While late Cretaceous North American climate remains unresolved (due to the uncertain influence of epicontinental seaways) (DeConto et al., 1999; Hay, 2017), it is accepted that temperatures were elevated and more equably distributed (Barron, 1983; Hallam, 1985), with poleward isotherm displacement (Barron, 1983). Atmospheric CO_2 concentrations are estimated to have been 4–10 times higher than preindustrial levels of 280 ppmv (see review by Wang et al. (2014)), with eustatic sea levels 100–200 m higher than present day (Haq et al., 1987) and an absence of permanent ice sheets (Savin et al., 1975; Shackleton & Kennett, 1975; Miller et al., 1999; Stoll & Schrag, 2000; Miller et al., 2003). As such, lack of permanent ice was conducive to the existence of major fluvial systems in Greenland (e.g. Pedersen & Pulvertaft, 1992; Jensen & Pedersen, 2010).

With a robust understanding of palaeogeography, extensive and well-documented exposures of Cretaceous strata, and a highly-refined chronology (Kauffman, 1977; Kauffman & Caldwell, 1993; Miall et al., 2008), the late Cretaceous North American continent, in particular the WIB, is an ideal natural laboratory for studying ancient source-to-sink systems and evaluating our approach.

3. Data sets and methods

3.1 Palaeogeographies and palaeoDEMs

PalaeoDEMs were provided by Getech Group Plc for Cenomanian and Turonian time slices (Table 1) and are *time-averaged* representations of palaeogeography and palaeotopography — palaeoDEMs are time-averaged across the entire length of the stage (see discussion in Markwick and Valdes (2004)). Each palaeoDEM comprises a single elevation raster with a spatial resolution of 0.1° latitude × 0.1° longitude, which equates to a cell size of ~11 × 11 km (Figure 1). Getech construct palaeoDEMs using the methodology of Markwick and Valdes (2004) and Markwick (2018), based on concepts developed by Ziegler et al. (1985). Getech palaeoDEMs have been used in a number of studies on pre-Quaternary palaeoclimate (e.g. Craggs et al., 2012; Hunter et al., 2013; Armstrong et al., 2016; Lunt et al., 2016; Tabor et al., 2016) and palaeo-sediment routing (Bonne, 2014).

Getech has generated an in-house global plate model, underpinned by knowledge of crustal architecture (i.e. the origin, composition and thickness of crust, as well as its structural framework) and geodynamic history, which is interpreted from data pertaining to igneous/sedimentary history, geochronology,

palaeomagnetism and structural geology. Tectonic blocks are assigned, each with unique geologic histories (including rift, drift and accretion histories) and unique rotation parameters; relative motions are calculated within the Global Hybrid Reference Frame of Torsvik et al. (2008). Other useful data, such as lithologic, palaeontologic or tectonic information are added into GIS compatible global databases. These are predominantly taken from the public domain and include data from publications, programmes (such as Deep Sea Drilling Project (DSDP) and Ocean Drilling Program (ODP)) and other sources, such as national geological surveys. Once collated these data are reconstructed back to their palaeo-coordinates using the plate model. These constraints are used to classify net-depositional environments and interpret contemporary base level, which separates net-depositional environments (below base level) and net-erosional, 'tectonophysiographic' terranes (above base level; see discussion of contemporary base level in Markwick and Valdes (2004)). This facilitates reconstruction of the relative distribution of relief. To reconstruct maximum elevation, Getech use analogue elevation distributions of modern tectonic settings and models of orogen growth and decay. In contrast, minimum elevation is reconstructed using depositional lithofacies and marine fossil occurrences to identify highstand palaeoshorelines (throughout this manuscript we refer to highstands and lowstands in terms of third- and fourth-order cycles, on 10^5–10^6 myr timescales). Getech use palaeodrainage information, where available, from sedimentologic, stratigraphic and provenance studies, to guide interpolation of base contours (minimum elevation, contemporary base level and maximum elevation) to an elevation raster. The end product is nine global, terrestrial contours that have been interpolated, using the palaeodrainage network, to an elevation raster with a cell size of 0.1° latitude × 0.1° longitude. For full, detailed information on palaeogeographic mapping workflow, see Markwick and Valdes (2004) and Markwick (2018).

3.2 HadCM3L GCM

HadCM3L GCM palaeoclimate data are time-averaged representations of Cenomanian and Turonian palaeoclimate, and include mean annual air temperature at 1.5 m above the local surface and mean annual precipitation (Figure 2). These data have a spatial resolution of 2.5° latitude × 3.75° longitude, which equates to a cell size of 278 × 417 km at the equator and 278 × 295 km at 45° latitude (Gordon et al., 2000; Hunter et al., 2008), and the same stage-length temporal resolution as the Cenomanian and Turonian palaeoDEMs.

Cenomanian and Turonian palaeoclimate data are identical to those presented and described in Farnsworth et al. (2019), with atmospheric CO_2 set at 1120 ppmv (×4 preindustrial atmospheric CO_2) and using Cenomanian and Turonian palaeoDEMs as boundary conditions. The model used is very similar to the HadCM3BLM2.1aD model that is described and evaluated under modern climate configuration in

Valdes et al. (2017), except that it includes a modification to the ozone profile which ensures that the model does not develop a runaway warming at ×4 preindustrial atmospheric CO_2, as discussed in Lunt et al. (2016). For further information on boundary conditions used in HadCM3L simulations see Supplementary Information S1 and Farnsworth et al. (2019). Additional information on HadCM3L boundary conditions, assumptions and experimental design in pre-Quaternary palaeoclimate modelling is discussed in Lunt et al. (2016).

3.3 Reconstructing palaeocatchments and extracting catchment geometries

We define the extent of the North American palaeo-continent as encompassing the palaeo-position of Greenland, Canada, U.S.A, Mexico and Central America. To reconstruct the size and distribution of Cenomanian and Turonian palaeocatchments, we analysed the two palaeoDEMs in ArcGIS 10.5.1 (using the hydrological toolbox) to establish large channel networks and delineate palaeocatchment boundaries (Figures 3 and 4; for a detailed ArcGIS workflow, see Supplementary Information S2). For each reconstructed palaeocatchment, we used zonal statistics to extract palaeocatchment geometries, which included drainage area (A) and maximum relief (R).

Interpolation between base contours during palaeoDEM construction results in low-lying areas adjacent to the palaeoshoreline that do not preserve relief (see Supplementary Information S2) — these palaeocatchments are mostly small with drainage areas ≤500km^2. At this point we therefore omitted palaeocatchments with drainage areas ≤500km^2 (as well as larger palaeocatchments with zero/negligible relief). Removed palaeocatchments make up 1.5–2% of the total continental area and do not impact modelled estimates of total continental *Qs* as, with zero/negligible relief, they recover zero/negligible *Qs* (Equation 1). Our investigations are therefore focused on large reconstructed palaeocatchments with drainage areas ≥500 km^2. Independently validating these ancient catchments for the whole Cenomanian and Turonian North American continent is impossible due to the incomplete geologic record; instead, we compare palaeocatchment geometries, where possible, with estimates of drainage area, provenance and palaeo-elevation (e.g Chase et al., 1998; DeCelles, 2004; DeCelles & Coogan, 2006) in published literature.

3.4 Reconstructing catchment palaeoclimate variables

Palaeoclimate data from HadCM3L were resampled to the spatial resolution of palaeoDEMs using a bilinear resampling technique (Figure 2). We then used zonal statistics to derive the catchment-averaged mean annual temperature (T) and mean annual precipitation (P) of each palaeocatchment.

We require mean annual water discharge (Q) of each palaeocatchment to estimate *Qs*. To estimate Q, we multiplied drainage area by modelled mean annual precipitation. This method is simple, repeatable and minimises assumptions in our approach — our water discharge values are therefore maximum estimates because they effectively assume that evaporation and storage is zero. Subsurface and surface runoff data are actually available from HadCM3L simulations (see Supplementary Information S3), which has a full hydrological cycle including precipitation, evaporation, and runoff. However, we are presenting a methodology in which we model input parameters, and we therefore need to be able to somewhat constrain or corroborate these values with geologic evidence. In some other applications only data for precipitation may be available (such as when precipitation is estimated from proxy records, e.g. White et al. (2001)); as such, here we use precipitation only. Nevertheless, we tested the sensitivity of using modelled subsurface and surface runoff data to estimate Q and *Qs* and we present these results in Supplementary Information S3. We suggest that use of subsurface and surface runoff data to estimate Q and *Qs* can be applied at catchment-scales where runoff-derived Q estimates can be corroborated by geological evidence (e.g. identification of catchment runoff class from geological indicators, as discussed in Eide et al. (2018)).

3.5 Comparison of palaeocatchments with modern catchments

We compared palaeotopography with modern topography to probe whether the palaeocatchment and palaeoclimate data that we extract are reasonable and in line with expectation, particularly the spread of data across the continent. To do this we used the same workflow to derive catchment geometries and catchment-averaged climate in the modern North American continent from ASTER and GTOPO30 global digital elevation models (GDEMs), decimated to the same 0.1° resolution as palaeoDEMs. We excluded Greenland (now ice-covered, but not during the Cretaceous) from comparison of palaeo- and modern topography. As we use smoothed and filled modern topographies, we included the GTOPO30 GDEM used to derive the USGS HYDRO1k database, which permits comparison of modelled drainage with actual drainage. To retrieve modern distributions of catchment-averaged climate, we used WorldClim mean annual temperature and total annual precipitation data sets, compiled from global weather stations between 1960–1990 and interpolated to a spatial resolution of 30 arc seconds, or 2.5, 5, and 10 arc minutes (see Hijmans et al. (2005)). WorldClim data sets are averaged over decadal time scales, which is consistent with HadCM3L experiment outputs.

For palaeo- and modern DEMs, we plotted the cumulative frequency of catchments relative to their drainage area, maximum relief, mean annual temperature, and mean annual precipitation, ordered from

smallest to largest in each instance. This facilitates comparison and additionally aids visualisation of the data that we extracted from palaeoDEMs and HadCM3L outputs.

3.6 BQART suspended sediment discharge model

We used BQART (Equations 1a and 1b) to predict time-averaged suspended sediment load, *Qs*, for all reconstructed palaeocatchments with areas ≥500 km^2 in the Cenomanian and Turonian North American continent. To implement BQART, we extracted A, R, T, and P (hence Q) for each palaeocatchment, as previously described. We set B equal to 1 in all analyses as it is not necessary to consider glacial and anthropogenic impact in the Cretaceous. While lithology is considered in B, Syvitski and Milliman (2007) indicate the global mean is 1, so for simplicity and to avoid the introduction of unconstrained variables we maintain this value here. We converted *Qs* from a suspended sediment load with units of megatonnes per year (MT/yr) to a suspended sediment discharge with units of cubic metres per year (m^3/yr). For this conversion we used a plausible sediment porosity of 40% and a sediment grain density of 2650 kg/m^3; unconsolidated sediments typically have a porosity of at least 40% (Manger, 1963) so we have used this as a minimum estimate. *Qs* would vary proportionally if a different porosity or grain density were known to be more appropriate for a regional/catchment-scale study. With *Qs* quoted in units of volume per unit of time, we did a straight volume shift and divided palaeocatchment *Qs* values by their respective drainage area values to calculate catchment-averaged erosion rates (i.e. catchment-averaged denudation rates) — they are therefore functionally equivalent to sediment yields. The workflow required to reconstruct *Qs* and catchment-averaged erosion rates from palaeoDEMs and GCM data is summarised diagrammatically in Figure 5.

With estimates of *Qs* and catchment-averaged erosion rate for Cenomanian and Turonian palaeocatchments, we mapped their spatial distributions across the North American continent. We also plotted north–south transects depicting latitudinal variations in *Qs* and catchment-averaged erosion rates along the western WIS margin. Latitudinal variations were assessed by dividing the western WIS margin into 5° latitudinal bins and calculating the sum of *Qs* and the mean catchment-averaged erosion rate for all catchments that drain to a catchment outflow point within the limits of a specified latitudinal bin.

3.7 Uncertainties and comparison with previous studies

A formal analysis of the uncertainty of palaeogeographic reconstructions is not possible because we cannot know the real palaeotopography, and because palaeogeographies are time-averaged. Subsequently, we compared our *Qs* estimates with published estimates for two sediment routing systems in the Cenomanian and Turonian that drained to the WIS:

i. Dunvegan delta

The middle Cenomanian Dunvegan Formation, Canada, represents the earliest appearance of southeast-flowing rivers that drained to the western WIS margin; the southeast-thinning clastic wedge contains palaeovalley systems which have been interpreted as representing a network of tributaries that merge to form trunk valleys (Plint, 2002; Plint & Wadsworth, 2003; Bhattacharya et al., 2016). The ancient trunk channel of the Dunvegan Formation is considered to have drained an area of order 10^5 km^2 (Bhattacharya et al., 2016; Lin & Bhattacharya, 2017); Lin and Bhattacharya (2017) used the channel palaeohydrologic approach of Holbrook and Wanas (2014) to estimate a mean annual *Qs* of 5.2×10^6 to 11.9×10^6 m^3 for this system.

ii. Ferron Notom delta

The middle Turonian Ferron Sandstone of Utah, USA, comprises three deltaic clastic wedges that were fed by rivers draining the Sevier orogenic belt to the western WIS margin, from which the Vernal, Last Chance, and Notom deltas have been described (Cotter, 1975) and extensively studied (see papers in volume edited by Chidsey et al. (2004)). Recent work has focused extensively on characterising channel geometries and hydrology in palaeochannels draining to the Ferron Notom delta (e.g Bhattacharyya et al., 2015; Kimmerle & Bhattacharya, 2018; Li et al., 2018); in particular, Sharma et al. (2017) also used the channel palaeohydrologic approach of Holbrook and Wanas (2014) to estimate a mean annual *Qs* of 1.5×10^6 to 4.4×10^6 m^3.

For comparison with published estimates, we identified the most plausible representative palaeocatchments in our model, based on published palaeolatitude, drainage area and palaeoflow direction, as well as palaeogeographic reconstructions (such as those reproduced in Bhattacharya et al. (2016)). We then compared BQART-derived estimates of *Qs* for our 'candidate' catchments with published estimates. We subsequently evaluated how uncertain our palaeogeographic and palaeoclimatic boundary conditions (P, hence Q, A, R and T) must be before BQART-derived estimates of *Qs* are inconsistent with published estimates of *Qs* from Lin and Bhattacharya (2017) and Sharma et al. (2017) respectively. We evaluated the univariate sensitivity of *Qs* values by applying 10%, 20%, 30%, 40% and 50% uncertainty margins to each parameter, one at a time. Then, we evaluated the multivariate sensitivity of *Qs* values by applying 10%, 20%, 30%, 40% and 50% uncertainty margins to all parameters at the same time. However, as temperature is a scale with an arbitrary zero value, we instead apply ±1°C, ±2°C, ±3°C, ±4°C and ±5°C uncertainty margins to mean annual temperature in sensitivity analyses. We contrasted ranges in *Qs*

values associated with univariate and multivariate sensitivity with minimum and maximum *Qs* values estimated by Lin and Bhattacharya (2017) and Sharma et al. (2017).

Beyond uncertainty in palaeogeographic and palaeoclimatic boundary conditions, we must also consider that palaeoDEMs depict highstand palaeoshorelines. In this study we do not change palaeogeographic boundary conditions to accommodate lowstand conditions as this requires information on lowstand catchment geometries, which are not well-known at continental scales, and would require that HadCM3L is re-run (changes to land–sea configurations could change local/regional climate). Instead, we consider the implication of this on a case-by-case basis using sensitivity results.

4. Results

4.1 Palaeocatchment geometries and palaeoclimate

For the North American continent, we reconstructed 1623 Cenomanian palaeocatchments and 1742 Turonian palaeocatchments with areas ≥500 km^2 (Supplementary Figure 1). Maximum drainage areas in the Cenomanian and Turonian are of order 990,000 km^2 and 830,000 km^2, respectively, which reflect large continental catchments comparable in size to drainage areas of the modern Rio Grande and Yukon rivers of North America (Milliman & Farnsworth, 2013). Palaeocatchment data are summarised in Tables 2 and 3 — note that these data include Greenland, whereas subsequent comparison of palaeo- and modern topography does not.

For catchment drainage areas, the 25th, 50th and 75th percentiles are all higher in the palaeo-continent than the modern continent; median drainage areas in the Cenomanian and Turonian are 2560 km^2 and 2750 km^2, respectively, whereas modern, smoothed DEMs recover median drainage areas of 1680 km^2 and 1570 km^2 (Figure 6a, Supplementary Table 2). This is expected as, in the absence of the WIS, modern North America is dominated by large, continental-scale drainage networks which results in a higher relative frequency of smaller catchments. For catchment maximum relief, the 25th percentile is higher in the modern continent than the palaeo-continent (Cenomanian = 59m, Turonian = 74m, modern = 153m or 172m; Figure 6b, Supplementary Table 2). This is likely due to interpolation of contours during palaeoDEM reconstruction which results in abundant low-lying catchments with low relief. Whereas, the 75th percentile is roughly three times higher in the palaeo-continent than in the modern continent (Cenomanian = 2280m, Turonian = 2270m, modern = 684m or 790m; Figure 6b, Supplementary Table 2). This is likely the result of land–sea configurations associated with the WIS which forced abundant catchments along the western WIS margin — these catchments all have high maximum relief associated with the Sevier orogenic fold-and-thrust belt.

For catchment mean annual temperatures the 25th, 50th and 75th percentiles are all higher in the palaeo-continent than the modern continent. Median catchment mean annual temperatures for the Cenomanian and Turonian are 11.5°C and 9.1°C, respectively, whereas modern DEMs and WorldClim data sets recover median values of 1.8°C and 0°C. Distributions converge toward the 75th percentile (Cenomanian = 19.2°C, Turonian = 17.5°C, modern = 16.3°C or 11.6°C; Figure 6c, Supplementary Table 2). Higher catchment mean annual temperatures in the palaeo-continent are consistent with a warmer, more equable late Cretaceous greenhouse climate (Farnsworth et al., 2019), rather than the modern icehouse climate. Narrower 10–90 percentile ranges for catchment mean annual temperatures in the palaeo-continent are also consistent with a more equable climate (Cenomanian = 23.3°C, Turonian = 26.3°C, modern = 39.2°C or 42.1°C). For catchment mean annual precipitation, the 25th percentile is higher in the palaeo-continent than the modern continent (Cenomanian = 617 mm/yr, Turonian = 572 mm/yr, modern = 227 mm/yr or 184 mm/yr) and distributions converge towards the 50th and 75th percentiles (Figure 6d, Supplementary Table 2). This is also consistent with a late Cretaceous greenhouse climate with intensified precipitation.

4.2 Comparison with published palaeocatchments and estimates of *Qs*

i. Case study 1: Dunvegan delta, Lin and Bhattacharya (2017)

Rivers draining the Cenomanian Dunvegan Formation had a palaeolatitude of ~65° (Bhattacharya et al., 2016) and an estimated drainage area of order 140,000–180,000 km^2 (Lin & Bhattacharya, 2017). We identify two plausible catchments, Dunvegan 1 (D1) and Dunvegan 2 (D2), in our model (Figure 4a) which lie at the correct palaeolatitude and could have sourced the sediments draining the Dunvegan system. Palaeocatchments D1 and D2 have areas of 113,200 km^2 and 123,400 km^2 respectively, similar to that predicted by Lin and Bhattacharya (2017). Based on channel-fill palaeohydrology the authors predicted a mean annual *Qs* of 5.2 x10^6 m^3 to 11.9 x10^6 m^3. We reconstruct *Qs* values of 6.6 x10^6 m^3/yr and 4.7 x10^6 m^3/yr for catchments D1 and D2, respectively. D1 *Qs* falls within the predicted range derived from geologic evidence, meanwhile D2 *Qs* is the same order of magnitude as, and within a factor of two of, the lower value of the predicted range.

ii. Case study 2: Ferron Notom delta, Sharma et al. (2017)

The Notom delta complex of the Turonian Ferron Sandstone had a palaeolatitude of ~45° (Bhattacharya et al., 2016) and is believed to have drained an area of order 10^4 km^2. Bhattacharya and Tye (2004) estimated that the drainage area for the Last Chance delta complex of the Ferron Sandstone was of order 50,000 km^2, with both the Vernal (relatively larger drainage area) and Notom (relatively smaller drainage area) delta complexes also draining an area 10^4 km^2. We identify two catchments with the correct

palaeolatitude and palaeoflow direction that could plausibly have drained to the Notom delta, Ferron Notom 1 (F1) and Ferron Notom 2 (F2), which drain areas of 26,000 km^2 and 11,100 km^2 respectively (Figure 4b). Sharma et al. (2017) similarly used channel-fill palaeohydrology to reconstruct *Qs* to the Ferron Notom delta and reconstructed a mean annual *Qs* of 1.5 $x10^6$ to 4.4 $x10^6$ m^3. We reconstructed *Qs* values of 9.7 $x10^6$ m^3/yr and 5.2 $x10^6$ m^3/yr for catchments F1 and F2, respectively. F1 and F2 *Qs* values are both greater than the predicted range derived from geologic evidence but, at maximum, within a factor of two to three of the upper value of the predicted range. Our *Qs* estimates are more consistent with the estimates of Sharma et al. (2017) when the smaller F2 catchment draining to the Ferron is assumed.

4.3 Sensitivity of our approach

Results from our two case studies suggest our approach produces plausible first-order estimates of *Qs*. However, it is important that we quantify the univariate and multivariate sensitivity of our *Qs* estimates to unknown uncertainties in palaeogeographic (A, R) and palaeoclimatic (P, T) boundary conditions (Figure 7).

i. Univariate and multivariate sensitivity in Dunvegan case study

We retrieve palaeogeographic and palaeoclimatic boundary conditions from our two candidate catchments, D1 and D2, for the Cenomanian Dunvegan Formation. In D1, A is 113,200 km^2, R is 4150 m, T is 3.4°C and P is 1090 mm/yr. Whereas in D2, A is 123,400 km^2, R is 4230 m, T is −0.6°C and P is 1430 mm/yr. In our univariate analysis, to obtain estimates of *Qs* that are either consistent with Lin & Bhattacharya's (2017) range, or within a factor of two bigger than the maximum bound/a factor of two smaller than the minimum bound of this range, we can apply uncertainty margins of 40–50% to A, R and P, or ±5°C to T, for both D1 and D2 (Figure 7a,c).

For our multivariate analysis, to retrieve estimates of *Qs* that are either consistent with Lin & Bhattacharya's (2017) range, or within a factor of two bigger/smaller than the maximum/minimum bounds of this range, we can apply uncertainty margins of up to 20–30%/±2–3°C to all parameters in D1 and D2 (Figure 7b,d). We also note that with 50%/±5°C uncertainty margins on all parameters, *Qs* estimates are still within one order of magnitude, and within a factor of five to six, of the author's maximum/minimum bounds for both D1 and D2 (Figure 7b,d).

ii. Univariate and multivariate sensitivity in Ferron case study

For the Turonian Ferron Sandstone, we also retrieve palaeogeographic and palaeoclimatic boundary conditions for our two candidate catchments, F1 and F2. In F1, A is 26,000 km^2, R is 4000 m, T is 14.9°C and P is 1580 mm/yr. Whereas in F2, A is 11,110 km^2, R is 4010 m, T is 16.4°C and P is 1470 mm/yr. For the univariate sensitivity analysis, to obtain estimates of *Qs* that are either consistent with the range predicted by Sharma et al. (2017), or within a factor of two bigger than the maximum bound/a factor of two smaller than the minimum bound of this range, we can apply uncertainty margins of 50% /±5°C to A, R , T and P in F2 (Figure 7g). Whereas for F1, these same uncertainty margins retrieve estimates of *Qs* that are within a factor of three to four bigger than the maximum bound (Figure 7e).

In our multivariate analysis, to retrieve estimates of *Qs* that are either consistent with the range that Sharma et al. (2017) predicted, or within a factor of two bigger than the maximum bound/a factor of two smaller than the minimum bound of this range, we can apply uncertainty margins of up to ~30%/±3°C to all parameters in F2 (Figure 7h), whereas in F1 these error margins recover estimates of *Qs* that are within a factor of ~four bigger than the maximum bound (Figure 7f). We also note that with 50%/±5°C uncertainty margins on all parameters, *Qs* estimates are still within one order of magnitude of the author's maximum and minimum bounds for both F1 and F2, and are within a factor of four for F2 and a factor of seven for F1 (Figure 7f,h).

Our case studies and sensitivity analyses suggest that our approach is suitable for making first-order approximations of *Qs* in ancient source-to-sink systems. In detail, uncertainty margins of up to 50%/±5°C on all palaeogeographic and palaeoclimatic boundary conditions still reconstruct *Qs* values that are within one order of magnitude of, and within a factor of four to seven of, published constraints. As expected analytically in BQART (Equation 1), we also observe that *Qs* estimates are least sensitive to uncertainties in precipitation estimates (which are multiplied by drainage area to estimate water discharge), and are more sensitive to uncertainty in temperature in cooler catchments than warmer catchments.

4.4 *Qs* and catchment-averaged erosion rates in the Cenomanian and Turonian North American continent

Assuming our approach has merit, we find that spatial distributions of *Qs* were highly variable across Cenomanian and Turonian North American catchments (Figure 8). During the Cenomanian, *Qs* spanned 7 orders of magnitude, up to 9.7 $x10^7$ m^3/yr with a median of 8.8 $x10^4$ m^3/yr (Figure 9). Whereas during the Turonian, *Qs* spanned 7 orders of magnitude up to 8.9 $x10^7$ m^3/yr with a median of 9.2 $x10^4$ m^3/yr (Figure 9). For the whole continent, we estimate total suspended sediment loads of 3.4 GT/yr and 3.2 GT/yr (or 1.8 $x10^9$ m^3/yr and 1.7 $x10^9$ m^3/yr) in the Cenomanian and Turonian, respectively.

Qs values demonstrate an overall increase towards low latitudes (Figure 8a,b), with high *Qs* values in large continental palaeocatchments, particularly in Appalachia and at high latitudes around Greenland. There is also a significant difference in total *Qs* input on either side of the WIS. We calculate that the western WIS margin contributes approximately three times more sediment to the WIS than the eastern margin. High *Qs* values in excess of 10^6 m^3/yr persist along the western WIS margin, whereas on the eastern margin high *Qs* values are only reconstructed in low latitude catchments that drain from the Appalachians to the Gulf of Mexico and the Atlantic.

Our results also imply that catchment-averaged erosion rates were highly variable across the Cenomanian and Turonian North American continent. Median catchment-averaged erosion rates of 0.02 mm/yr, and average catchment-averaged erosion rates of 0.1 mm/yr, are obtained for the Cenomanian and Turonian, with maximum catchment-averaged erosion rates of 0.8 mm/yr and 0.9 mm/yr for the two time intervals, respectively.

Similar to *Qs*, catchment-averaged erosion rates increase towards low latitudes (Figure 8c,d); this increase is pronounced on the western margin of the WIS, whereas on the eastern margin they remain low (<0.2 mm/yr), except in low latitude catchments draining from the Appalachians to the Atlantic, and sparse catchments draining to the Gulf of Mexico. However, erosion rate trends are discrepant with *Qs* trends in large continental palaeocatchments where *Qs* values are high (>10^6 m^3/yr at high latitudes and >10^7 m^3/yr at low latitudes) yet catchment-averaged erosion rates are low (<0.2 mm/yr).

While there are small differences in the spatial variation of *Qs* and catchment-averaged erosion rates between the Cenomanian and Turonian, we find that distributions of catchments relative to *Qs* and catchment-averaged erosion rate are almost identical for both time slices (Figure 9).

4.5 Latitudinal trends in *Qs* and catchment-averaged erosion rates along the western WIS margin

Following observed latitudinal variability in sediment supply across the continent, north–south transects along the western WIS margin (Figure 10) offer more refined observations. We predict that export of sediment to the western WIS margin is lowest at high latitudes and increases towards mid-latitudes, with maximum sediment export between 35°N and 40°N in both the Cenomanian and Turonian. For the Cenomanian, *Qs* values increase by a factor of five, from 1.8 x10^7 m^3/yr at 65–70°N to 9.5 x10^7 m^3/yr at 35–40°N. Whereas for the Turonian, *Qs* values increase by a factor of 22, from 4.9 x10^6 m^3/yr at 70–75°N to 1.1 x10^8 m^3/yr at 35–40°N. After *Qs* peaks at 35–40°N, *Qs* is projected to decrease by less than a factor of two towards low latitudes (20–25°N) in both the Cenomanian and Turonian. Catchment-averaged erosion rates increase from north to south, with maximum catchment-averaged erosion rates at the

southernmost tip of the continent, between 20°N and 25°N, and an additional smaller peak between 50°N and 60°N (Figure 10c,d). For both the Cenomanian and Turonian, catchment-averaged erosion rates increase north to south by just over one order of magnitude, from 0.05 mm/yr at 65–70°N to 0.57 mm/yr at 20–25°N in the Cenomanian, and from 0.04 mm/yr at 70–75°N to 0.48 mm/yr at 20–25°N in the Turonian.

The sensitivity of north–south latitudinal trends to uncertainty is also illustrated (Figure 10). The presented uncertainty margins are based on adoption of 10%/±1°C uncertainty on all boundary conditions; it is impossible to know the actual uncertainties, but we note that it is not possible to make all palaeocatchments 20% or 30% larger, or increase the relief of all catchments by similar margins, without producing unrealistic values for the size and elevations of the North American continent. The most notable effect of adopting 10%/±1°C uncertainty on trends is that sensitivity is not uniform along the north–south latitudinal transect. Sensitivity increases towards low latitudes; *Qs* and catchment-averaged erosion rates are most sensitive to uncertainty at mid- to low latitudes, between 20° and 45° where mean annual temperature and mean annual precipitation are higher, which is expected analytically (see Equations 1a and 1b).

5. Discussion

Are reconstructed palaeocatchments reasonable? What are the wider uncertainties of this approach?

Are our reconstructions of continental drainage in the late Cretaceous realistic? Along the western WIS margin, a north–south trending drainage divide associated with the Sevier orogenic belt separates short steep catchments that drain to the Pacific Ocean and short steep catchments that drain to the WIS. Of catchments that drain to the WIS, their configurations are consistent with several well-studied ancient source-to-sink systems. These include published palaeogeographic reconstructions of fluvial systems that fed the Dunvegan Formation, Alberta, Canada (e.g Plint & Wadsworth, 2003, 2006), the Cardium Formation, Alberta (e.g. Krause et al., 1994), the Vernal, Last Chance and Notom deltaic complexes of the Ferron Sandstone, Utah (e.g. Cotter, 1975), the Frontier Formation, Wyoming, USA, the Kaiparowits Formation, Utah, and the Gallup Sandstone, New Mexico (see Bhattacharya et al. (2016) and references therein).

On the eastern WIS margin, the Appalachian drainage divide separates short steep catchments that drain to the Atlantic and larger continental-scale catchments that drain to the eastern WIS margin and Hudson Seaway. The Woodbine Formation, Texas, and Tuscaloosa Formation, Alabama–Mississippi, represent southwestward drainage from the Appalachians to the Gulf of Mexico (Adams & Carr, 2010; Blum et al.,

2017) — this is consistent with palaeocatchments that we reconstruct for this region. Moreover, our palaeocatchment configurations on the eastern WIS margin are consistent with published models of large continental drainages, which have been inferred from studies of the Dakota Sandstone, western Iowa and eastern Nebraska, where analysis of detrital zircons indicates continental-scale drainage from the Appalachians to the WIS (Finzel, 2014) (Figure 3). While we do not expect our reconstructed palaeocatchments to be in any way a perfect representation of palaeodrainage, we conclude that, to first order, their configurations are reasonable (Figure 3; Supplementary Figure 1).

One limitation of our reconstructed palaeocatchments is that they are derived from palaeoDEMs that represent highstand conditions, which is typical practice in palaeoDEM construction for purposes of hydrocarbon exploration (Markwick, 2018). In this study we compare our *Qs* estimates with constraints from the Dunvegan Formation and Ferron Sandstone. However, the Dunvegan Formation was deposited at lowstand conditions when the palaeoshoreline likely advanced (Roberts & Kirschbaum, 1995); at lowstand conditions we expect drainage length to increase, and we also expect drainage area to increase as low-lying rivers coalesce. This has been observed extensively in Quaternary studies, such that rivers in northwest Europe (e.g. Thames, Rhine) were formerly tributaries of the lowstand Channel River that drained westward through the English Channel to the Atlantic (e.g. Gibbard, 1988; Lericolais et al., 2003). The implication of this is that our estimates of drainage area from the palaeoDEM, and therefore estimates of *Qs*, are underpredicted. We consider the implications of this on *Qs* estimates using results of our univariate sensitivity analyses where we showed that increasing drainage area up to ~50% and beyond renders *Qs* values that are still consistent with published field constraints (Figure 7a,c). It is also entirely possible that palaeocatchments D1 and D2 (Section 4.2) could have coalesced at lowstand to feed the Dunvegan deltas. The combined sediment discharge of D1 and D2 is 11.3 $x10^6$ m^3/yr (which is still consistent with the range of values estimated by Lin and Bhattacharya (2017)) so, with a greater drainage area at lowstand, we may expect sediment discharges to be greater than this, but perhaps of the same order. Conversely, during the Turonian, the palaeoshoreline in central Utah remained in a relative highstand position, despite sea level change, which has been attributed to local subsidence keeping pace with rates of sediment accumulation (Roberts & Kirschbaum, 1995). This supports use of a highstand palaeoDEM to estimate *Qs* to the Ferron depocentre. Drainage capture or episodic sediment transport from different source regions may also lead to underprediction of drainage area. For example, in Utah, provenance studies on strata both time-correlative and younger/older than the Ferron Sandstone have suggested intermittent sourcing from the Mogollon Highlands (Arizona) and Cordilleran magmatic arc to the south (Owen et al., 2015; Szwarc et al., 2015; Bartschi et al., 2018; Primm et al., 2018), which may also

potentially be true for the Ferron. These examples highlight the necessity of considering the implications of highstand palaeoshorelines and drainage areas on a case-by-case basis, in conjunction with sensitivity analyses, where the interest is in catchment/regional scale studies. At minimum, palaeoDEMs with highstand palaeoshorelines will recover estimates of minimum *Qs.*

Wider uncertainties in palaeocatchment configurations and drainage areas are centred on uncertainty in the position of palaeoshorelines and drainage divides in palaeoDEMs, as well as the palaeodrainage used to interpolate contours in palaeoDEM construction. Meanwhile, sources of uncertainty in maximum relief include the position and height of the maximum elevation contour in palaeoDEMs. To expand further, the two main sources of error in HadCM3L simulations, and therefore catchment-averaged temperature and precipitation estimates, are centred on the model itself (the magnitude of which can be estimated by assessing the model's ability to represent modern climate, as in Valdes et al. (2017)) and the model boundary conditions which, for the timescales addressed here, are centred on the prescribed atmospheric CO_2 concentration and the palaeoDEM used (for further discussion refer to Supplementary Information S1). Assessing the likely uncertainty should be tackled on a case-by-case basis at regional/catchment scales using knowledge of the likely sources and magnitudes of uncertainty, geologic evidence and sensitivity results. We advise that, given unknown uncertainties and the current spatio-temporal resolution of data, but with consistency with published estimates and reasonably (and increasingly) advanced knowledge of palaeotopography, *Qs* estimates can be considered first-order estimates that are likely precise to within one order of magnitude.

How suitable is BQART for ancient source-to-sink analysis?

Application of BQART to ancient source-to-sink systems requires constraints on palaeocatchment drainage area, maximum relief, mean annual temperature and mean annual precipitation, and a defined B factor. Syvitski and Milliman (2007) showed that when B is set to 1, BQART explains 66% of variance in *Qs* in modern systems, whereas when B is adjusted to reflect glacial, anthropogenic and lithologic conditions, BQART explains 96% of variance. However, BQART was originally developed from a modern global river data set (n=488) in which glacial coverage and anthropogenic activity, e.g. artificial sediment trapping and land use, are ubiquitous. Glacial coverage and anthropogenic activity are both major controls on *Qs* (e.g. Hallet et al., 1996; Syvitski et al., 2005) and are accounted for by Syvitski and Milliman (2007) in B. So, while setting B to 1 results in BQART explaining 66% of variance in *Qs* in modern systems, we might expect it to explain more variance in ancient systems, especially in the Cretaceous where glacial coverage and anthropogenic activity do not control *Qs*. However, this is difficult to test with data sets of modern source-to-sink systems as most large global rivers are affected by anthropogenic activity.

Having used BQART to estimate *Qs* in the Cenomanian and Turonian North American continent, there are, of course, issues to consider when validating BQART-derived *Qs* estimates with published constraints. BQART is used to estimate suspended load, which typically comprises silts and fine sands; this varies in global rivers, however, as many rivers may carry coarser grade sands in suspension. In this study we compare BQART-derived *Qs* estimates with published estimates from systems in which sands may or may not have been carried in suspension — depositional stratigraphy can be used to constrain mode of sediment transport in individual instances (Lin & Bhattacharya, 2017; Sharma et al., 2017). Moreover, while BQART estimates suspended load, bedload is also a potentially significant component of fluvial sediment discharge (Turowski et al., 2010). However, bedload fractions are difficult to constrain in modern systems, let alone ancient systems, and the empirical basis of various methods is often derived from small data sets (e.g. Schlunegger & Hinderer, 2003; Syvitski & Saito, 2007). One influence that inability to constrain bedload will have on our results is that catchment-averaged erosion rates are underpredicted.

Any comparison of BQART-derived *Qs* estimates with published constraints implicitly assumes that the previously published *Qs* estimates are robust themselves. In this study we use constraints derived from channel-fill palaeohydrology — this approach is not exact, with uncertainties centred on flow transport calculations (see Holbrook & Wanas, 2014). Nevertheless, the ability to recover estimates that are consistent with field data highlights potential to use BQART to make first-order approximations, particularly where we do not have access to outcrop data or where the geologic record is incomplete. In fact, if we assume published constraints are correct, then BQART estimates that are consistent with, or within a factor of two to three of, these constraints should be considered a successful result.

Suspended sediment discharges in the Cenomanian and Turonian North American continent

We estimate total continental *Qs* of 3.4 GT/yr and 3.2 GT/yr (or 1.8 x10^9 m^3/yr and 1.7 x10^9 m^3/yr) in the Cenomanian and Turonian, respectively. This implies that total continental *Qs* was a factor of two bigger in the Cenomanian and Turonian North American continent than the modern continent, when compared with Holocene pre-anthropogenic continental *Qs* estimates of 1.7 GT/yr (Syvitski & Kettner, 2011), which were similarly derived using BQART. Further, we are comparing total continental *Qs* during the ancient Zuñi sequence highstand with the current Tejas sequence lowstand (in this specific instance we instead are referring to longer, second-order cycles, on 10^7–10^8 myr timescales) — we are not just predicting that twice as much sediment exported to oceans, we are also implying that it was exported from half of the land. Therefore, sediment yields (T/ km^2/yr) in the Cenomanian and Turonian North American continent may have been up to four times greater than today.

We find that *Qs* is highly variable across the North American continent, spanning seven orders of magnitude (in units of m^3/yr). The western WIS margin is an important source of sediment along its entire north–south transect, and generally increases towards low latitudes (which is likely due to increased mean annual precipitation towards the tropics). However, we note that BQART is more sensitive to uncertainty in palaeogeographic and palaeoclimatic boundary conditions at mid- to low latitudes. Whereas, the eastern WIS margin is only an important source of sediment at low latitudes in catchments draining southwestward from the Appalachians to the Gulf of Mexico.

Catchment-averaged erosion rates increase towards low latitudes — however we expect these values to be an underprediction as bedload is not accounted for. Further, when we consider our catchment-averaged erosion rates, we expect source-area denudation rates to be higher as we focus on large catchments in which sediment trapping in low-lying areas is expected to be prominent. Painter et al. (2014) used AFT ages and DZ analysis to estimate local erosion rates >1 mm/yr in the Sevier orogenic fold-and-thrust belt, western U.S.A, whereas we reconstruct maximum catchment-averaged erosion rates of 0.5–0.6 mm/yr along the U.S.A portion of the western WIS margin.

Our estimates and spatial distributions of *Qs* and catchment-averaged erosion rates offer opportunities to exploit new lines of enquiry in the Cretaceous North American continent. In conjunction with palaeogeographic reconstructions, our results can be considered in the context of the long-term carbon cycle and organic carbon burial where, generally speaking, the efficiency of organic carbon burial is greater in small, active margin systems than large, passive margin systems (Blair et al., 2004; Leithold et al., 2016). Other avenues to consider include chemical weathering and nutrient fluxes in systems where source rock lithologies are known — recent work suggests an important link between palaeogeography and global weatherability throughout the Phanerozoic (Kent & Muttoni, 2013; Goddéris et al., 2017; Macdonald et al., 2019). Moreover, we have provided first-order estimates of Cenomanian and Turonian palaeodrainage networks (Figure 3), which is useful to field geologists interested in conducting regional source-to-sink studies. These opportunities are associated with the spatial and temporal scale of this study; extrapolation of our approach to different spatial and temporal scales offers further opportunities, but also requires adaptation to minimise uncertainties.

The future: opportunities and suitability of our approach at different spatial and temporal scales

We consider our approach suitable for making first-order approximations of *Qs* at continental scales. However, targeted interest in reconstructing *Qs* at catchment/regional scales requires further efforts to constrain palaeogeographic and palaeoclimatic boundary conditions using geological evidence, or to

calibrate *Qs* estimates with field data. Results of our univariate sensitivity analyses highlight advantages of constraining boundary conditions using geological evidence, where possible, however we acknowledge that the feasibility of this decreases as spatial scale increases. We suggest that, for catchment/regional scales, palaeocatchment configurations and geometries should be augmented by published provenance analyses, where chronometric techniques such as U–Pb ages of detrital zircons are used to identify and characterise source areas (e.g. Blum & Pecha, 2014; Spencer et al., 2014). Moreover, estimates of maximum relief in palaeocatchments may potentially be refined, or supported, using stable-isotope based palaeoaltimetry (e.g Chamberlain & Poage, 2000; Rowley et al., 2001; Rowley & Currie, 2006; Rowley & Garzione, 2007).

To refine catchment-averaged palaeoclimate at catchment/regional scales, water discharge and mean annual temperature estimates can be supported using Cretaceous climate zone maps deduced from large palaeontological, sedimentological and mineralogical data sets (Chumakov et al., 1995), which have since been reproduced (Skelton et al., 2003; Hay & Floegel, 2012). Also, where broad estimates of palaeoclimate can be inferred from preservation of climatically-sensitive sediments etc., water discharge can be estimated using drainage area and one of four runoff categories, following Eide et al. (2018). Beyond water discharge estimates, constraints on catchment-averaged temperature might be inferred from terrestrial surface temperature proxies (see Supplementary Information S1).

PalaeoDEMs offer time-averaged "snapshots" of palaeogeography and palaeotopography (Markwick & Valdes, 2004) so are well-suited to investigation of long-period forcings (but require careful consideration if investigating short-period, high-frequency forcings). We consider change across time slices to represent broad change in *Qs* and catchment-averaged erosion rates on multimillion, 10^6–10^7, year timescales, which reflects environmental signals associated with long-period forcings such as orogenic cycles, uplift and major shifts in global climate (Allen, 2008b; Romans et al., 2016). Long-period forcings are recorded in palaeogeographic reconstructions by changes to continental configurations and changes to elevation associated with orogenic growth and decay, which, as boundary conditions, then affect output of HadCM3L climate simulations (Markwick & Valdes, 2004; Markwick, 2018).

Incorporation of more time slices into analyses could expand the temporal scale of investigation to 10^7–10^8 yr timescales, which would additionally reflect environmental signals associated with supercontinental cycles, i.e. the effect of changing land–sea configurations as ocean basins open and close (Wilson, 1966). Moreover, at this temporal scale it is possible to capture signals associated with global shift from greenhouse to icehouse climate states, such as transition from Cretaceous–Eocene greenhouse conditions

to Oligocene–present icehouse conditions (e.g Zachos et al., 2008). However, investigation on 10^7–10^8 yr timescales requires adaptation of HadCM3L boundary conditions (see Supplementary Information S1) to reflect coeval changes to atmospheric CO_2 and other greenhouse gases before, during and after major climatic shifts (Foster et al., 2017). This ensures that palaeoclimate reconstructed by HadCM3L, using palaeoDEMs as boundary conditions, is not solely driven by changing palaeogeography. Other climatic forcings that may be captured as temporal (and spatial) scale increases include the supercontinent effect; previous studies suggest that supercontinents likely featured arid interiors with much larger interannual temperature ranges than present (Crowley et al., 1987; Crowley et al., 1989), these ranges being more closely related to solar forcing than ocean forcing (Otto-Bliesner & Houghton, 1986), and that monsoonal climates were likely restricted to coastal regions (Kutzbach et al., 1993).

Other opportunities associated with expanding temporal scale include investigation of provenance during WIB evolution. Our spatial variations in *Qs* on either side of the WIS are consistent with models of foreland basin evolution, in which the western WIS margin (fold-and-thrust belt) contributes more sediment than the eastern margin (stable continental craton). However, work in the northern Andean foreland basin demonstrates that sediment derived from the stable continental craton might be an important source of sediment during early foreland basin evolution (Horton et al., 2010a; Horton et al., 2010b), which could also be explored during WIB evolution using appropriate Cretaceous palaeogeographic time slices.

Conversely, it may be possible to narrow the temporal scale of analysis by changing palaeogeographic and palaeoclimatic boundary conditions associated with each time slice to accommodate highstand vs. lowstand conditions, where fully understood, or rapid continental-scale palaeodrainage reorganisation (e.g. Galloway et al., 2011) . In particular, palaeoclimatic boundary conditions could be tweaked in line with published constraints to explore changes in *Qs* and catchment-averaged erosion rates over orbital cycles or periods of environmental change, such as the Cenomanian–Turonian oceanic anoxic event (OAE) or the Cretaceous–Paleogene (K–Pg) extinction event.

6. Conclusions

We evaluated high-resolution palaeogeographic reconstructions as a first-order investigative tool in palaeo-sediment routing system analysis. We used palaeoDEMs, HadCM3L data and BQART to estimate palaeodrainage networks, *Qs* and catchment-averaged erosion rates in the Cenomanian and Turonian North American continent, and our results show that:

(1) The palaeocatchment geometries and climates that we reconstructed are reasonable compared to palaeogeographic reconstructions of ancient source-to-sink systems in published literature, as well as the distributions of catchment geometries and climates in the modern North American continent.

(2) Our BQART-derived *Qs* estimates are consistent with published constraints for the Cenomanian Dunvegan Formation in Alberta, Canada, and the Turonian Ferron Sandstone in Utah, USA. Our estimates are the same order of magnitude as, and are either consistent or within a factor of two to three of, published estimates in both instances.

(3) Univariate sensitivity of BQART to palaeogeographic and palaeoclimatic boundary conditions supports use of our approach at catchment scales. It also highlights the potential to use geological evidence, where available, to refine palaeogeographic or palaeoclimatic boundary conditions and minimise uncertainty.

(4) Multivariate sensitivity of BQART to palaeogeographic and palaeoclimatic boundary conditions demonstrates that, despite unquantifiable uncertainties associated with palaeogeographic reconstructions, our approach can be used to make first-order approximations of *Qs*. We found that adoption of large uncertainties (≤50%/±5°C) for all palaeogeographic and palaeoclimatic boundary conditions recovers BQART-derived *Qs* estimates that are still within an order of magnitude of, and within a factor of four to seven of, published constraints.

(5) *Qs* and catchment-averaged erosion rates are highly variable across the Cenomanian and Turonian North American continent, with overall increase towards low latitudes. Moreover, the western WIS margin may have contributed three times more suspended sediment to the WIS than the eastern margin.

(6) Total continental *Qs* may have been up to a factor of two bigger in the Cenomanian and Turonian stages than estimates of Holocene pre-anthropogenic continental *Qs*. This invites investigation regarding the relative role of palaeogeographic change and major climate shifts in determining continental *Qs* over 10^7–10^8 yr time scales.

Our results demonstrate that high-resolution palaeogeographies can be used to make first-order approximations of fluvial suspended sediment discharges in the geologic past on a variety of spatial and temporal scales, and will be particularly useful where stratigraphic records are incomplete. However, we stress that calibration with geological evidence, where possible, is crucial to minimising uncertainty. Moreover, we highlight the potential to use this approach to address some of the grand challenges in the

geosciences, such as the global spatio-temporal response of *Qs* and catchment-averaged erosion rates to long-period tectonic and climatic forcing in the geologic past.

Data availability

ASTER, GTOPO30 and WorldClim data used in this study are freely available online; ASTER GDEM and GTOPO30 DEM can be obtained from https://asterweb.jpl.nasa.gov/gdem.asp and https://earthexplorer.usgs.gov/, and WorldClim data can be obtained from https://www.worldclim.org/. The HadCM3L climate model output is available from https://www.paleo.bristol.ac.uk/ummodel/scripts/papers/Farnsworth_et_al_2019.html. For more information on Getech palaeoDEMs, and how to obtain them, contact Getech Group Plc (https://getech.com/globe/).

References

Adams, R. L., & Carr, J. P. (2010). Regional depositional systems of the Woodbine, Eagle Ford, and Tuscaloosa of the U.S. Gulf Coast. *Gulf Coast Association of Geological Societies Transactions, 60*, 3-27.

Allen, P. A. (2008a). From landscapes into geological history. *Nature, 451*, 274-276. doi:10.1038/nature06586

Allen, P. A. (2008b). Time scales of tectonic landscapes and their sediment routing systems. *Geological Society, London, Special Publications, 296*(1), 7-28. doi:10.1144/sp296.2

Allen, P. A., Armitage, J. J., Carter, A., Duller, R. A., Michael, N. A., Sinclair, H. D., . . . Whittaker, A. C. (2013). The *Qs* problem: Sediment volumetric balance of proximal foreland basin systems. *Sedimentology, 60*(1), 102-130. doi:10.1111/sed.12015

Armitage, J. J., Duller, R. A., Whittaker, A. C., & Allen, P. A. (2011). Transformation of tectonic and climatic signals from source to sedimentary archive. *Nature Geoscience, 4*(4), 231-235. doi:10.1038/ngeo1087

Armstrong, H. A., Wagner, T., Herringshaw, L. G., Farnsworth, A. J., Lunt, D. J., Harland, M., . . . Atar, E. F. L. (2016). Hadley circulation and precipitation changes controlling black shale deposition in the Late Jurassic Boreal Seaway. *Paleoceanography, 31*(8), 1041-1053. doi:10.1002/2015PA002911

Armstrong, R. L. (1968). Sevier Orogenic Belt in Nevada and Utah. *GSA Bulletin, 79*(4), 429-458. doi:10.1130/0016-7606(1968)79[429:SOBINA]2.0.CO;2

Barron, E. J. (1983). A warm, equable Cretaceous: The nature of the problem. *Earth-Science Reviews, 19*(4), 305-338. doi:10.1016/0012-8252(83)90001-6

Bartschi, N. C., Saylor, J. E., Lapen, T. J., Blum, M. D., Pettit, B. S., & Andrea, R. A. (2018). Tectonic controls on Late Cretaceous sediment provenance and stratigraphic architecture in the Book Cliffs, Utah. *GSA Bulletin, 130*(11-12), 1763-1781. doi:10.1130/B31927.1

Benyon, C., Leier, A., Leckie, D. A., Webb, A., Hubbard, S. M., & Gehrels, G. (2014). Provenance of the Cretaceous Athabasca Oil Sands, Canada: Implications for continental-scale sediment transport. *Journal of Sedimentary Research, 84*(2), 136-143. doi:10.2110/jsr.2014.16

Bernard, C. Y., Dürr, H. H., Heinze, C., Segschneider, J., & Maier-Reimer, E. (2011). Contribution of riverine nutrients to the silicon biogeochemistry of the global ocean – a model study. *Biogeosciences, 8*(3), 551-564. doi:10.5194/bg-8-551-2011

Beusen, A. H. W., Bouwman, A. F., Dürr, H. H., Dekkers, A. L. M., & Hartmann, J. (2009). Global patterns of dissolved silica export to the coastal zone: Results from a spatially explicit global model. *Global Biogeochemical Cycles, 23*(4), GB0A02. doi:10.1029/2008GB003281

Bhattacharya, J., & Tye, B. (2004). Searching for modern Ferron analogs and application to subsurface interpretation. In T. C. Chidsey Jr., R. D. Adams, & T. H. Morris (Eds.), *Regional to Wellbore Analog for Fluvial-Deltaic Reservoir Modeling: The Ferron Sandstone of Utah* (pp. 39-57): AAPG Studies in Geology 50, 39-57.

Bhattacharya, J. P., Copeland, P., Lawton, T. F., & Holbrook, J. (2016). Estimation of source area, river paleo-discharge, paleoslope, and sediment budgets of linked deep-time depositional systems and implications for hydrocarbon potential. *Earth-Science Reviews, 153*, 77-110. doi:10.1016/j.earscirev.2015.10.013

Bhattacharyya, P., Bhattacharya, J. P., & Khan, S. D. (2015). Paleo-channel reconstruction and grain size variability in fluvial deposits, Ferron Sandstone, Notom Delta, Hanksville, Utah. *Sedimentary Geology, 325*, 17-25. doi:10.1016/j.sedgeo.2015.05.001

Blair, N. E., Leithold, E. L., & Aller, R. C. (2004). From bedrock to burial: the evolution of particulate organic carbon across coupled watershed-continental margin systems. *Marine Chemistry, 92*(1), 141-156. doi:10.1016/j.marchem.2004.06.023

Blum, M., & Pecha, M. (2014). Mid-Cretaceous to Paleocene North American drainage reorganization from detrital zircons. *Geology, 42*, 607-610. doi:10.1130/G35513.1

Blum, M. D., Milliken, K. T., Pecha, M. A., Snedden, J. W., Frederick, B. C., & Galloway, W. E. (2017). Detrital-zircon records of Cenomanian, Paleocene, and Oligocene Gulf of Mexico drainage integration and sediment routing: Implications for scales of basin-floor fans. *Geosphere, 13*(6), 2169–2205. doi:10.1130/GES01410.1

Bonne, K. P. M. (2014). Reconstruction of the evolution of the Niger River and implications for sediment supply to the Equatorial Atlantic margin of Africa during the Cretaceous and the Cenozoic. *Geological Society, London, Special Publications, 386*(1), 327-349. doi:10.1144/sp386.20

Boyden, J. A., Müller, R. D., Gurnis, M., Torsvik, T. H., Clark, J. A., Turner, M., . . . Cannon, J. S. (2011). Next-generation plate-tectonic reconstructions using GPlates. In *Geoinformatics: Cyberinfrastructure for the Solid Earth Sciences* (Vol. 9, pp. 95-113): Cambridge University Press.

Brenner, R. L., Ludvigson, G. A., Witzke, B. L., Phillips, P. L., White, T. S., Ufnar, D. F., . . . Shirk, B. R. (2003). Aggradation of gravels in tidally influenced fluvial systems: upper Albian (Lower Cretaceous) on the cratonic margin of the North American Western Interior foreland basin. *Cretaceous Research, 24*(4), 439-448. doi:10.1016/s0195-6671(03)00054-5

Carvajal, C., & Steel, R. (2012). Source-to-sink sediment volumes within a tectono-stratigraphic model for a Laramide shelf-to-deep-water basin: methods and results. In C. Busby & A. Azor (Eds.), *Tectonics of Sedimentary Basins: Recent Advances* (pp. 131-151): Blackwell Publishing Ltd.

Cederbom, C. E., van der Beek, P., Schlunegger, F., Sinclair, H. D., & Oncken, O. (2011). Rapid extensive erosion of the North Alpine foreland basin at 5–4 Ma. *Basin Research, 23*(5), 528-550. doi:10.1111/j.1365-2117.2011.00501.x

Chamberlain, C. P., & Poage, M. A. (2000). Reconstructing the paleotopography of mountain belts from the isotopic composition of authigenic minerals. *Geology, 28*, 115-118. doi:10.1130/0091-7613(2000)28<115:RTPOMB>2.0.CO;2

Chase, C. G., Gregory-Wodzicki, K. M., Parrish, J. T., & DeCelles, P. G. (1998). Topographic history of the Western Cordillera of North America and controls on climate. In T. J. Crowley & K. Burke (Eds.), *Tectonic Boundary Conditions for Climate Reconstructions* (Vol. 39, pp. 73-99): Oxford Monographs on Geology and Geophysics.

Chiarenza, A. A., Mannion, P. D., Lunt, D. J., Farnsworth, A., Jones, L. A., Kelland, S.-J., & Allison, P. A. (2019). Ecological niche modelling does not support climatically-driven dinosaur diversity decline before the Cretaceous/Paleogene mass extinction. *Nature Communications, 10*(1), 1091. doi:10.1038/s41467-019-08997-2

Chidsey, T. C., Adams, R. D., & Morris, T. H. (2004). *Regional to Wellbore Analog for Fluvial-Deltaic Reservoir Modeling: The Ferron Sandstone of Utah* (Vol. 50).

Chumakov, N. M., Zharkov, M. A., Herman, A. B., Doludenko, M. P., Kalandadze, N. N., Lebedev, E. A., . . . Rautian, A. S. (1995). Climate belts of the mid-Cretaceous time. *Stratigraphy and Geological Correlation, 3*, 42-63.

Cohen, S., Kettner, A. J., Syvitski, J. P. M., & Fekete, B. M. (2013). WBMsed, a distributed global-scale riverine sediment flux model: Model description and validation. *Computers & Geosciences, 53*(Supplement C), 80-93. doi:10.1016/j.cageo.2011.08.011

Cotter, E. (1975). Deltaic deposits in the Upper Cretaceous Ferron Sandstone, Utah. In M. L. Broussard (Ed.), *Deltas: Models for Exploration* (pp. 471-484): Houston Geological Society.

Craggs, H. J., Valdes, P. J., & Widdowson, M. (2012). Climate model predictions for the latest Cretaceous: An evaluation using climatically sensitive sediments as proxy indicators. *Palaeogeography, Palaeoclimatology, Palaeoecology, 315-316*(Supplement C), 12-23. doi:10.1016/j.palaeo.2011.11.004

Cross, T. A. (1986). Tectonic controls of foreland basin subsidence and Laramide style deformation, western United States. In P. A. Allen & P. Homewood (Eds.), *Foreland Basins* (Vol. 8, pp. 15-39): International Association of Sedimentologists Special Publication.

Crowley, T. J., Hyde, W. T., & Short, D. A. (1989). Seasonal cycle variations on the supercontinent of Pangaea. *Geology, 17*(5), 457-460. doi:10.1130/0091-7613(1989)017<0457:SCVOTS>2.3.CO;2

Crowley, T. J., Mengel, J. G., & Short, D. A. (1987). Gondwanaland's seasonal cycle. *Nature, 329*, 803-807. doi:10.1038/329803a0

DeCelles, P. G. (1994). Late Cretaceous–Paleocene synorogenic sedimentation and kinematic history of the Sevier thrust belt, northeast Utah and southwest Wyoming. *GSA Bulletin, 106*, 32-56. doi:10.1130/0016-7606(1994)106<0032:LCPSSA>2.3.CO;2

DeCelles, P. G. (2004). Late Jurassic to Eocene evolution of the Cordilleran thrust belt and foreland basin system, western U.S.A. *American Journal of Science - AMER J SCI, 304*. doi:10.2475/ajs.304.2.105

DeCelles, P. G., & Coogan, J. C. (2006). Regional structure and kinematic history of the Sevier fold-and-thrust belt, central Utah. *GSA Bulletin, 118*(7/8), 841-864. doi:10.1130/B25759.1

DeConto, R. M., Hay, W. W., Thompson, S. L., & Bergengren, J. (1999). Late Cretaceous climate and vegetation interactions: Cold continental interior paradox. In E. Barrera & C. C. Johnson (Eds.), *Evolution of the Cretaceous Ocean-Climate System* (Vol. 332, pp. 0): Geological Society of America.

Duller, R. A., Whittaker, A. C., Fedele, J. J., Whitchurch, A. L., Springett, J., Smithells, R., . . . Allen, P. A. (2010). From grain size to tectonics. *Journal of Geophysical Research: Earth Surface, 115*(F3), F03022. doi:10.1029/2009JF001495

Dürr, H. H., Meybeck, M., Hartmann, J., Laruelle, G. G., & Roubeix, V. (2011). Global spatial distribution of natural riverine silica inputs to the coastal zone. *Biogeosciences, 8*(3), 597-620. doi:10.5194/bg-8-597-2011

Eide, C. H., Müller, R., & Helland-Hansen, W. (2018). Using climate to relate water discharge and area in modern and ancient catchments. *Sedimentology, 65*(4), 1378-1389. doi:10.1111/sed.12426

Farnsworth, A., Lunt, D. J., O'Brien, C., Foster, G. L., Inglis, G. N., Markwick, P., . . . Robinson, S. A. (2019). Climate sensitivity on geological timescales controlled by non-linear feedbacks and ocean circulation. *Geophysical Research Letters, 0*(ja). doi:10.1029/2019GL083574

Fedele, J. J., & Paola, C. (2007). Similarity solutions for fluvial sediment fining by selective deposition. *Journal of Geophysical Research: Earth Surface, 112*(F2), F02038. doi:10.1029/2005JF000409

Finzel, E. S. (2014). Detrital zircons from Cretaceous midcontinent strata reveal an Appalachian Mountains–Cordilleran foreland basin connection. *Lithosphere, 6*(5), 378-382. doi:10.1130/L400.1

Foster, G. L., Royer, D. L., & Lunt, D. J. (2017). Future climate forcing potentially without precedent in the last 420 million years. *Nature Communications, 8*, 14845. doi:10.1038/ncomms14845

Galloway, W. E., Whiteaker, T. L., & Ganey-Curry, P. (2011). History of Cenozoic North American drainage basin evolution, sediment yield, and accumulation in the Gulf of Mexico basin. *Geosphere, 7*(4), 938-973. doi:10.1130/ges00647.1

Garvin, M. G. (2008). Late quaternary geochronologic, stratigraphic, and sedimentologic framework of the Trinity River incised valley: east Texas coast. *LSU Master's Theses*, 1122.

Gibbard, P. L. (1988). The history of the great northwest European rivers during the past three million years. *Philosophical Transactions of the Royal Society B: Biological Sciences, 318*(1191), 559-602. doi:10.1098/rstb.1988.0024

Goddéris, Y., Donnadieu, Y., Carretier, S., Aretz, M., Dera, G., Macouin, M., & Regard, V. (2017). Onset and ending of the late Palaeozoic ice age triggered by tectonically paced rock weathering. *Nature Geoscience, 10*, 382. doi:10.1038/ngeo2931

Gordon, C., Cooper, C., Senior, C. A., Banks, H., Gregory, J. M., Johns, T. C., . . . Wood, R. A. (2000). The simulation of SST, sea ice extents and ocean heat transports in a version of the Hadley Centre coupled model without flux adjustments. *Climate Dynamics, 16*(2), 147-168. doi:10.1007/s003820050010

Hallam, A. (1985). A review of Mesozoic climates. *Journal of the Geological Society, 142*(3), 433-445. doi:10.1144/gsjgs.142.3.0433

Hallet, B., Hunter, L., & Bogen, J. (1996). Rates of erosion and sediment evacuation by glaciers: A review of field data and their implications. *Global and Planetary Change, 12*(1), 213-235. doi:10.1016/0921-8181(95)00021-6

Hampson, G. J., Duller, R. A., Petter, A. L., Robinson, R. A. J., & Allen, P. A. (2014). Mass-balance constraints on stratigraphic interpretation of linked alluvial–coastal–shelfal deposits from source

to sink: example from Cretaceous Western Interior Basin, Utah and Colorado, U.S.A. *Journal of Sedimentary Research, 84*(11), 935-960. doi:10.2110/jsr.2014.78

Haq, B. U., Hardenbol, J. A. N., & Vail, P. R. (1987). Chronology of fluctuating sea levels since the Triassic. *Science, 235*(4793), 1156-1167. doi:10.1126/science.235.4793.1156

Hay, W., L. Eicher, D., & Diner, R. (1993). Physical oceanography and water masses of the Cretaceous Western Interior Seaway. In W. E. G. Caldwell & E. G. Kauffman (Eds.), *Evolution of the Western Interior Basin* (pp. 297-318): Geological Association of Canada.

Hay, W. W. (2017). Toward understanding Cretaceous climate — an updated review. *Science China Earth Sciences, 60*(1), 5-19. doi:10.1007/s11430-016-0095-9

Hay, W. W., DeConto, R. M., Wold, C. N., Wilson, K. M., Voigt, S., Schulz, M., . . . Söding, E. (1999). Alternative global Cretaceous paleogeography. In E. Barrera & C. C. Johnson (Eds.), *Evolution of the Cretaceous Ocean-Climate System*: Geological Society of America.

Hay, W. W., & Floegel, S. (2012). New thoughts about the Cretaceous climate and oceans. *Earth-Science Reviews, 115*(4), 262-272. doi:10.1016/j.earscirev.2012.09.008

Helland-Hansen, W., Sømme, T., Martinsen, O. J., Lunt, I., & Thurmond, J. (2016). Deciphering Earth's natural hourglasses: perspectives on source-to-sink analysis. *Journal of Sedimentary Research, 86*, 1008-1033. doi:10.2110/jsr.2016.56

Hidy, A. J., Gosse, J. C., Blum, M. D., & Gibling, M. R. (2014). Glacial–interglacial variation in denudation rates from interior Texas, USA, established with cosmogenic nuclides. *Earth and Planetary Science Letters, 390*, 209-221. doi:10.1016/j.epsl.2014.01.011

Hijmans, R. J., Cameron, S. E., Parra, J. L., Jones, P. G., & Jarvis, A. (2005). Very high resolution interpolated climate surfaces for global land areas. *International Journal of Climatology, 25*(15), 1965-1978. doi:10.1002/joc.1276

Holbrook, J., & Wanas, H. (2014). A fulcrum approach to assessing source-to-sink mass balance using channel paleohydrologic paramaters derivable from common fluvial data sets with an example from the Cretaceous of Egypt. *Journal of Sedimentary Research, 84*(5), 349-372. doi:10.2110/jsr.2014.29

Horton, B., Parra, M., Saylor, J., Nie, J., Mora, A., Torres, V., . . . Strecker, M. (2010a). Resolving uplift of the Northern Andes using detrital zircon age signatures. *GSA Today, 20*, 4-9. doi:10.1130/GSATG76A.1

Horton, B., Saylor, J., Nie, J., Mora, A., Parra, M., Reyes-Harker, A., & Stockli, D. (2010b). Linking sedimentation in the northern Andes to basement configuration, Mesozoic extension, and

Cenozoic shortening: Evidence from detrital zircon U-Pb ages, Eastern Cordillera, Colombia. *GSA Bulletin, 122*, 1423-1442. doi:10.1130/B30118.1

Hunter, S. J., Haywood, A. M., Valdes, P. J., Francis, J. E., & Pound, M. J. (2013). Modelling equable climates of the Late Cretaceous: Can new boundary conditions resolve data–model discrepancies? *Palaeogeography, Palaeoclimatology, Palaeoecology, 392*, 41-51. doi:10.1016/j.palaeo.2013.08.009

Hunter, S. J., Valdes, P. J., Haywood, A. M., & Markwick, P. J. (2008). Modelling Maastrichtian climate: investigating the role of geography, atmospheric CO2 and vegetation. *Climate of the Past Discussions, 4*, 981–1019. doi:10.5194/cpd-4-981-2008

Jensen, M. A., & Pedersen, G. K. (2010). Architecture of vertically stacked fluvial deposits, Atane Formation, Cretaceous, Nuussuaq, central West Greenland. *Sedimentology, 57*, 1280-1314. doi:10.1111/j.1365-3091.2010.01146.x

Jordan, T. E. (1981). Thrust loads and foreland basin evolution, Cretaceous, western United States. *AAPG Bulletin, 65*(12), 2506-2520.

Kauffman, E. G. (1977). Geological and biological overview: Western Interior Basin In E. G. Kauffman (Ed.), *Cretaceous facies, faunas, and paleoenvironments across the Western Interior Basin* (pp. 75-99): Rocky Mountain Association of Geologists.

Kauffman, E. G., & Caldwell, W. (1993). The Western Interior Basin in space and time. In E. G. Kauffman & W. Caldwell (Eds.), *Evolution of the Western Interior Basin: Geological Association of Canada, Special Paper 39* (pp. 1-30).

Kent, D. V., & Muttoni, G. (2013). Modulation of Late Cretaceous and Cenozoic climate by variable drawdown of atmospheric pCO_2 from weathering of basaltic provinces on continents drifting through the equatorial humid belt. *Climate of the Past, 9*(2), 525-546. doi:10.5194/cp-9-525-2013

Kimmerle, S., & Bhattacharya, J. P. (2018). Facies, backwater limits, and paleohydraulic analysis of rivers in a forced-regressive, compound incised valley, Cretaceous Ferron Sandstone, Utah, U.S.A. *Journal of Sedimentary Research, 88*(2), 177-200. doi:10.2110/jsr.2018.5

Krause, F., Deutsch, K. B., Joiner, S. D., Barclay, J., Hall, R. L., & Hills, L. V. (1994). Cretaceous Cardium Formation of the Western Canada sedimentary basin. In G. D. Mossop & I. Shetson (Eds.), *Geological Atlas of the Western Canada Sedimentary Basin. Canadian Society of Petroleum Geologists and Alberta Research Council* (pp. 485-511).

Kutzbach, J., Prell, W., & Ruddiman, W. (1993). Sensitivity of Eurasian climate to surface uplift of the Tibetan Plateau. *The Journal of Geology, 101*(2), 177-190. doi:10.1086/648215

Leithold, E. L., Blair, N. E., & Wegmann, K. W. (2016). Source-to-sink sedimentary systems and global carbon burial: A river runs through it. *Earth-Science Reviews, 153*, 30-42. doi:10.1016/j.earscirev.2015.10.011

Lericolais, G., Auffret, J. P., & Bourillet, J. F. (2003). The Quaternary Channel River: seismic stratigraphy of its palaeo-valleys and deeps. *Journal of Quaternary Science, 18*, 245-260. doi:10.1002/jqs.759

Li, Y., Bhattacharya, J. P., Ahmed, S., & Garza, D. (2018). Re-evaluating the paleogeography of the river-dominated and wave-influenced Ferron Notom Delta, Southern Central Utah: an integration of detailed facies-architecture and paleocurrent analysis. *Journal of Sedimentary Research, 88*(2), 214-240. doi:10.2110/jsr.2018.9

Lin, W., & Bhattacharya, J. P. (2017). Estimation of source-to-sink mass balance by a fulcrum approach using channel paleohydrologic parameters of the Cretaceous Dunvegan Formation, Canada. *Journal of Sedimentary Research, 87*(1), 97-116. doi:10.2110/jsr.2017.1

Liu, S., & Nummedal, D. (2004). Late Cretaceous subsidence in Wyoming: Quantifying the dynamic component. *Geology, 32*(5), 397-400. doi:10.1130/G20318.1

Liu, S., Nummedal, D., & Gurnis, M. (2014). Dynamic versus flexural controls of Late Cretaceous Western Interior Basin, USA. *Earth and Planetary Science Letters, 389*, 221-229. doi:10.1016/j.epsl.2014.01.006

Liu, S., Nummedal, D., & Liu, L. (2011). Migration of dynamic subsidence across the Late Cretaceous United States Western Interior Basin in response to Farallon plate subduction. *Geology, 39*(6), 555-558. doi:10.1130/G31692.1

Lunt, D., Farnsworth, A., Loptson, C., Foster, G., Markwick, P., O'Brien, C., . . . Wrobel, N. (2016). Palaeogeographic controls on climate and proxy interpretation. *Climate of the Past, 12*, 1181-1198. doi:10.5194/cpd-11-5683-2015

Lunt, D. J., Ross, I., Hopley, P. J., & Valdes, P. J. (2007). Modelling Late Oligocene C4 grasses and climate. *Palaeogeography, Palaeoclimatology, Palaeoecology, 251*(2), 239-253. doi:10.1016/j.palaeo.2007.04.004

Macdonald, F. A., Swanson-Hysell, N. L., Park, Y., Lisiecki, L., & Jagoutz, O. (2019). Arc-continent collisions in the tropics set Earth's climate state. *Science, 364*(6436), 181. doi:10.1126/science.aav5300

Manger, G. E. (1963). Porosity and bulk density of sedimentary rocks. *Geological Survey Bulletin, 1144-E*.

Markwick, P. J. (2018). Palaeogeography in exploration. *Geological Magazine, 156*, 366-407. doi:10.1017/S0016756818000468

Markwick, P. J., & Valdes, P. J. (2004). Palaeo-digital elevation models for use as boundary conditions in coupled ocean–atmosphere GCM experiments: a Maastrichtian (late Cretaceous) example.

Palaeogeography, Palaeoclimatology, Palaeoecology, 213(1-2), 37-63. doi:10.1016/j.palaeo.2004.06.015

Miall, A. D., Catuneanu, O., Vakarelov, B. K., & Post, R. (2008). The Western Interior Basin. In A. D. Miall (Ed.), *Sedimentary Basins of the World* (Vol. 5, pp. 329-362): Elsevier.

Michael, N. A., Whittaker, A. C., Carter, A., & Allen, P. A. (2014). Volumetric budget and grain-size fractionation of a geological sediment routing system: Eocene Escanilla Formation, south-central Pyrenees. *GSA Bulletin, 126*(3-4), 585-599. doi:10.1130/B30954.1

Miller, K. G., Barrera, E., Olsson, R. K., Sugarman, P. J., & Savin, S. M. (1999). Does ice drive early Maastrichtian eustasy? *Geology, 27*(9), 783-786. doi:10.1130/0091-7613(1999)027<0783:DIDEME>2.3.CO;2

Miller, K. G., Sugarman, P. J., Browning, J. V., Kominz, M. A., Hernández, J. C., Olsson, R. K., . . . Van Sickel, W. (2003). Late Cretaceous chronology of large, rapid sea-level changes: Glacioeustasy during the greenhouse world. *Geology, 31*(7), 585-588. doi:10.1130/0091-7613(2003)031<0585:LCCOLR>2.0.CO;2

Milliman, J. D., & Farnsworth, K. L. (2013). *River Discharge to the Coastal Ocean: A Global Synthesis*: Cambridge University Press.

Molnar, P., & England, P. (1990). Late Cenozoic uplift of mountain ranges and global climate change: chicken or egg? *Nature, 346*, 29-23. doi:10.1038/346029a0

Otto-Bliesner, B. L., & Houghton, D. D. (1986). Sensitivity of the seasonal climate of a general circulation model to ocean surface conditions and solar forcing. *Journal of Geophysical Research, 91*, 6682-6694. doi:10.1029/JD091iD06p06682

Owen, A., Jupp, P., Nichols, G., Hartley, A., Weissmann, G., & Sadykova, D. (2015). Statistical estimation of the position of an apex: Application to the geological record. *Journal of Sedimentary Research, 85*, 142-152. doi:10.2110/jsr.2015.16

Painter, C. S., Carrapa, B., DeCelles, P. G., Gehrels, G. E., & Thomson, S. N. (2014). Exhumation of the North American Cordillera revealed by multi-dating of Upper Jurassic–Upper Cretaceous foreland basin deposits. *GSA Bulletin, 126*(11/12), 1439-1464. doi:10.1130/B30999.1

Pang, M., & Nummedal, D. (1995). Flexural subsidence and basement tectonics of the Cretaceous Western Interior basin, United States. *Geology, 23*(2), 173-176. doi:10.1130/0091-7613(1995)023<0173:FSABTO>2.3.CO;2

Paul, J. D., Roberts, G. G., & White, N. (2014). The African landscape through space and time. *Tectonics, 33*(6), 898-935. doi:10.1002/2013TC003479

Pedersen, G. K., & Pulvertaft, T. C. R. (1992). The nonmarine Cretaceous of the West Greenland Basin, onshore West Greenland. *Cretaceous Research, 13*(3), 263-272. doi:10.1016/0195-6671(92)90002-8

Pelletier, J. D. (2012). A spatially distributed model for the long-term suspended sediment discharge and delivery ratio of drainage basins. *Journal of Geophysical Research: Earth Surface, 117*(F2), 1-15. doi:10.1029/2011JF002129

Petter, A. L., Steel, R. J., Mohrig, D., Kim, W., & Carvajal, C. (2013). Estimation of the paleoflux of terrestrial-derived solids across ancient basin margins using the stratigraphic record. *GSA Bulletin, 125*, 578-593. doi:10.1130/B30603.1

Pettit, B. S., Blum, M., Pecha, M., McLean, N., Bartschi, N. C., & Saylor, J. E. (2019). Detrital-Zircon U-Pb Paleodrainage Reconstruction and Geochronology of the Campanian Blackhawk–Castlegate Succession, Wasatch Plateau and Book Cliffs, Utah, U.S.A. *Journal of Sedimentary Research, 89*(4), 273-292. doi:10.2110/jsr.2019.18

Plint, A. G. (2002). Paleovalley systems in the Upper Cretaceous Dunvegan Formation, Alberta and British Columbia. *Bulletin of Canadian Petroleum Geology, 50*(2), 277-296. doi:10.2113/50.2.277

Plint, A. G., & Wadsworth, J. A. (2003). Sedimentology and palaeogeomorphology of four large valley systems incising delta plains, western Canada Foreland Basin: implications for mid-Cretaceous sea-level changes. *Sedimentology, 50*(6), 1147-1186. doi:10.1111/j.1365-3091.2003.00599.x

Plint, A. G., & Wadsworth, J. A. (2006). Delta-plain paleodrainage patterns reflect small-scale fault movement and subtle forebulge uplift: Upper Cretaceous Dunvegan Formation, Western Canada Foreland Basin. In R. W. Dalrymple, D. A. Leckie, & R. W. Tillman (Eds.), *Incised Valleys in Time and Space* (Vol. 85, pp. 0): SEPM Society for Sedimentary Geology.

Pope, V. D., Gallani, M. L., Rowntree, P. R., & Stratton, R. A. (2000). The impact of new physical parametrizations in the Hadley Centre climate model: HadAM3. *Climate Dynamics, 16*(2), 123-146. doi:10.1007/s003820050009

Primm, J. W., Johnson, C. L., & Stearns, M. (2018). Basin-axial progradation of a sediment supply driven distributive fluvial system in the Late Cretaceous southern Utah foreland. *Basin Research, 30*(2), 249-278. doi:10.1111/bre.12252

Roberts, L. N. R., & Kirschbaum, M. A. (1995). Paleogeography and the Late Cretaceous of the Western Interior of middle North America: coal distribution and sediment accumulation. *U.S. Geological Survey Professional Paper, 1561*, 1-65. doi:10.3133/pp1561

Romans, B. W., Castelltort, S., Covault, J. A., Fildani, A., & Walsh, J. P. (2016). Environmental signal propagation in sedimentary systems across timescales. *Earth-Science Reviews, 153*, 7-29. doi:10.1016/j.earscirev.2015.07.012

Romans, B. W., & Graham, S. A. (2013). A deep-time perspective of land-ocean linkages in the sedimentary record. *Annual Review of Marine Science, 5*, 69-94. doi:10.1146/annurev-marine-121211-172426

Rowley, D. B., & Currie, B. S. (2006). Palaeo-altimetry of the late Eocene to Miocene Lunpola basin, central Tibet. *Nature, 439*, 677-681. doi:10.1038/nature04506

Rowley, D. B., & Garzione, C. N. (2007). Stable isotope-based paleoaltimetry. *Annual Review of Earth and Planetary Sciences, 35*(1), 463-508. doi:10.1146/annurev.earth.35.031306.140155

Rowley, D. B., Pierrehumbert, R. T., & Currie, B. S. (2001). A new approach to stable isotope-based paleoaltimetry: implications for paleoaltimetry and paleohypsometry of the High Himalaya since the Late Miocene. *Earth and Planetary Science Letters, 188*(1), 253-268. doi:10.1016/S0012-821X(01)00324-7

Sadler, P. M. (1981). Sediment accumulation rates and the completeness of stratigraphic sections. *The Journal of Geology, 89*, 569-584. doi:10.1086/628623

Savin, S. M., Douglas, R. G., & Stehli, F. G. (1975). Tertiary marine paleotemperatures. *GSA Bulletin, 86*(11), 1499-1510. doi:10.1130/0016-7606(1975)86<1499:TMP>2.0.CO;2

Schlunegger, F., & Hinderer, M. (2003). Pleistocene/Holocene climate change, re-establishment of fluvial drainage network and increase in relief in the Swiss Alps. *Terra Nova, 15*(2), 88-95. doi:10.1046/j.1365-3121.2003.00469.x

Shackleton, N. J., & Kennett, J. P. (1975). Paleotemperature history of the Cenozoic and the initiation of Antarctic glaciation: oxygen and carbon isotope analyses in DSDP Sites 277, 279, and 281. *Initial reports of the Deep Sea Drilling Project 29*, 743-755. doi:10.2973/dsdp.proc.29.1975

Sharma, S., Bhattacharya, J. P., & Richards, B. (2017). Source-to-sink sediment budget analysis of the Cretaceous Ferron Sandstone, Utah, U.S.A., using the fulcrum approach. *Journal of Sedimentary Research, 87*(6), 594-608. doi:10.2110/jsr.2017.23

Skelton, P. W., Spicer, R. A., Kelley, S. P., & Gilmour, I. (2003). *The Cretaceous World*. Cambridge: Cambridge University Press.

Sømme, T. O., Helland-Hansen, W., Martinsen, O. J., & Thurmond, J. B. (2009). Relationships between morphological and sedimentological parameters in source-to-sink systems: a basis for predicting semi-quantitative characteristics in subsurface systems. *Basin Research, 21*(4), 361-387. doi:10.1111/j.1365-2117.2009.00397.x

Sømme, T. O., Martinsen, O. J., & Lunt, I. (2013). Linking offshore stratigraphy to onshore paleotopography: The Late Jurassic–Paleocene evolution of the south Norwegian margin. *GSA Bulletin, 125*(7-8), 1164-1186. doi:10.1130/B30747.1

Sømme, T. O., Piper, D. J. W., Deptuck, M. E., & Helland-Hansen, W. (2011). Linking onshore–offshore sediment dispersal in the Golo source-to-sink system (Corsica, France) during the late Quaternary. *Journal of Sedimentary Research, 81*(2), 118-137. doi:10.2110/jsr.2011.11

Spencer, C. J., Prave, A. R., Cawood, P. A., & Roberts, N. M. W. (2014). Detrital zircon geochronology of the Grenville/Llano foreland and basal Sauk Sequence in west Texas, USA. *GSA Bulletin, 126*(7-8), 1117-1128. doi:10.1130/B30884.1

Stephenson, S. N., Roberts, G. G., Hoggard, M. J., & Whittaker, A. C. (2014). A Cenozoic uplift history of Mexico and its surroundings from longitudinal river profiles. *Geochemistry, Geophysics, Geosystems, 15*(12), 4734-4758. doi:10.1002/2014GC005425

Stoll, H. M., & Schrag, D. P. (2000). High-resolution stable isotope records from the Upper Cretaceous rocks of Italy and Spain: Glacial episodes in a greenhouse planet? *GSA Bulletin, 112*(2), 308-319. doi:10.1130/0016-7606(2000)112<308:HSIRFT>2.0.CO;2

Syvitski, J. P., & Kettner, A. (2011). Sediment flux and the Anthropocene. *Philosophical Transactions of the Royal Society A: Mathematical, Physical and Engineering Sciences, 369*(1938), 957-975. doi:10.1098/rsta.2010.0329

Syvitski, J. P., Vörösmarty, C. J., Kettner, A. J., & Green, P. (2005). Impact of humans on the flux of terrestrial sediment to the global coastal ocean. *Science, 308*(5720), 376-380. doi:10.1126/science.1109454

Syvitski, J. P. M., & Milliman, J. D. (2007). Geology, geography, and humans battle for dominance over the delivery of fluvial sediment to the coastal ocean. *The Journal of Geology, 115*(1), 1-19. doi:10.1086/509246

Syvitski, J. P. M., & Saito, Y. (2007). Morphodynamics of deltas under the influence of humans. *Global and Planetary Change, 57*(3-4), 261-282. doi:10.1016/j.gloplacha.2006.12.001

Szwarc, T. S., Johnson, C. L., Stright, L. E., & McFarlane, C. M. (2015). Interactions between axial and transverse drainage systems in the Late Cretaceous Cordilleran foreland basin: Evidence from detrital zircons in the Straight Cliffs Formation, southern Utah, USA. *GSA Bulletin, 127*(3-4), 372-392. doi:10.1130/B31039.1

Tabor, C. R., Poulsen, C. J., Lunt, D. J., Rosenbloom, N. A., Otto-Bliesner, B. L., Markwick, P. J., . . . Feng, R. (2016). The cause of Late Cretaceous cooling: A multimodel-proxy comparison. *Geology, 44*(11), 963-966. doi:10.1130/g38363.1

Tindall, J., Flecker, R., Valdes, P., Schmidt, D. N., Markwick, P., & Harris, J. (2010). Modelling the oxygen isotope distribution of ancient seawater using a coupled ocean–atmosphere GCM: Implications for reconstructing early Eocene climate. *Earth and Planetary Science Letters, 292*(3-4), 265-273. doi:10.1016/j.epsl.2009.12.049

Tinker, J., de Wit, M., & Brown, R. (2008). Mesozoic exhumation of the southern Cape, South Africa, quantified using apatite fission track thermochronology. *Tectonophysics, 455*(1-4), 77-93. doi:10.1016/j.tecto.2007.10.009

Torsvik, T. H., Müller, R. D., Van der Voo, R., Steinberger, B., & Gaina, C. (2008). Global plate motion frames: toward a unified model. *Reviews of Geophysics, 46*(3), RG3004. doi:10.1029/2007RG000227

Turowski, J. M., Rickenmann, D., & Dadson, S. J. (2010). The partitioning of the total sediment load of a river into suspended load and bedload: a review of empirical data. *Sedimentology, 57*(4), 1126-1146. doi:10.1111/j.1365-3091.2009.01140.x

Valdes, P. J., Armstrong, E., Badger, M. P. S., Bradshaw, C. D., Bragg, F., Crucifix, M., . . . Williams, J. H. T. (2017). The BRIDGE HadCM3 family of climate models: HadCM3@Bristol v1.0. *Geoscientific Model Development, 10*(10), 3715-3743. doi:10.5194/gmd-10-3715-2017

Vernon, A. J., van der Beek, P. A., Sinclair, H. D., & Rahn, M. K. (2008). Increase in late Neogene denudation of the European Alps confirmed by analysis of a fission-track thermochronology database. *Earth and Planetary Science Letters, 270*(3-4), 316-329. doi:10.1016/j.epsl.2008.03.053

Walford, H., White, N., & Sydow, J. (2005). Solid sediment load history of the Zambezi Delta. *Earth and Planetary Science Letters, 238*(1-2), 49-63. doi:10.1016/j.epsl.2005.07.014

Wang, Y., Huang, C.-m., Sun, B., Quan, C., Wu, J., & Lin, Z. (2014). Paleo-CO_2 variation trends and the Cretaceous greenhouse climate. *Earth-Science Reviews, 129*, 136–147. doi:10.1016/j.earscirev.2013.11.001

Watkins, S. E., Whittaker, A. C., Bell, R. E., McNeill, L. C., Gawthorpe, R. L., Brooke, S. A. S., & Nixon, C. W. (2018). Are landscapes buffered to high-frequency climate change? A comparison of sediment fluxes and depositional volumes in the Corinth Rift, central Greece, over the past 130 k.y. *GSA Bulletin, 131*, 372-388. doi:10.1130/B31953.1

Whipple, K., & Meade, B. (2006). Orogen response to changes in climatic and tectonic forcing. *Earth and Planetary Science Letters, 243*(1-2), 218-228. doi:10.1016/j.epsl.2005.12.022

Whipple, K. X. (2009). The influence of climate on the tectonic evolution of mountain belts. *Nature Geoscience, 2*(2), 97-104. doi:10.1038/ngeo413

White, T., González, L., Ludvigson, G., & Poulsen, C. (2001). Middle Cretaceous greenhouse hydrologic cycle of North America. *Geology, 29*(4), 363-366. doi:10.1130/0091-7613(2001)029<0363:MCGHCO>2.0.CO;2

Whittaker, A. C. (2012). How do landscapes record tectonics and climate? *Lithosphere, 4*(2), 160-164. doi:10.1130/rf.l003.1

Whittaker, A. C., Attal, M., & Allen, P. A. (2010). Characterising the origin, nature and fate of sediment exported from catchments perturbed by active tectonics. *Basin Research, 22*(6), 809-828. doi:10.1111/j.1365-2117.2009.00447.x

Whittaker, A. C., Duller, R. A., Springett, J., Smithells, R. A., Whitchurch, A. L., & Allen, P. A. (2011). Decoding downstream trends in stratigraphic grain size as a function of tectonic subsidence and sediment supply. *GSA Bulletin, 123*(7-8), 1363-1382. doi:10.1130/B30351.1

Willett, S. D. (1999). Orogeny and orography: The effects of erosion on the structure of mountain belts. *Journal of Geophysical Research: Solid Earth, 104*(B12), 28957-28981. doi:10.1029/1999jb900248

Wilson, J. T. (1966). Did the Atlantic close and then re-open? *Nature, 211*, 676-681. doi:10.1038/211676a0

Witzke, B. J., & Ludvigson, G. A. (1994). The Dakota Formation in Iowa and the type area. In G. W. Shurr, G. A. Ludvigson, & R. H. Hammond (Eds.), *Perspectives on the Eastern Margin of the Cretaceous Western Interior Basin* (Vol. 287): The Geological Society of America.

Witzke, B. J., Ludvigson, G. A., Poppe, J. R., & Ravn, R. L. (1983). Cretaceous paleogeography along the eastern margin of the Western Interior Seaway, Iowa, southern Minnesota, and eastern Nebraska and South Dakota. *Mesozoic Paleogeography of the West-Central United States: Rocky Mountain Symposium, 2*, 225-252.

Wobus, C., Whipple, K. X., Kirby, E., Snyder, N., Johnson, J., Spyropolou, K., . . . Sheehan, D. (2006). Tectonics from topography: Procedures, promise, and pitfalls. In S. D. Willett, N. Hovius, M. T. Brandon, & D. M. Fisher (Eds.), *Tectonics, Climate, and Landscape Evolution*: Geological Society of America.

Zachos, J. C., Dickens, G. R., & Zeebe, R. E. (2008). An early Cenozoic perspective on greenhouse warming and carbon-cycle dynamics. *Nature, 451*, 279-283. doi:10.1038/nature06588

Zhang, J., Covault, J., Pyrcz, M., Sharman, G., Carvajal, C., & Milliken, K. (2018). Quantifying sediment supply to continental margins: Application to the Paleogene Wilcox Group, Gulf of Mexico. *AAPG Bulletin, 102*(9), 1685-1702. doi:10.1306/01081817308

Ziegler, A. M., Rowley, D. B., Lottes, A. L., Sahagian, D. L., Hulver, M. L., & Gierlowski, T. C. (1985). Paleogeographic interpretation: With an example from the mid-Cretaceous. *Annual Review of Earth and Planetary Sciences, 13*(1), 385-428. doi:10.1146/annurev.ea.13.050185.002125

Table 1: Durations of Cenomanian and Turonian stages and the reconstruction ages of their associated palaeo-digital elevation models (palaeoDEMs).

Table 2: A summary of catchment geometries in Cenomanian and Turonian North American palaeocatchments, derived from analysis of palaeo-digital elevation models (palaeoDEMs). These data include Greenland.

Table 3: A summary of catchment-averaged palaeoclimate in Cenomanian and Turonian North American palaeocatchments, derived from analysis of palaeo-digital elevation models (palaeoDEMs) and HadCM3L general circulation model (GCM) data. These data include Greenland.

Figure 1: Onshore palaeo-digital elevation models (palaeoDEMs) for the Cenomanian (part **A**) and Turonian (part **B**) North American continent. Key palaeogeographic features are labelled, including the Sevier orogenic highlands, Laramidian landmass, Western Interior Seaway (WIS), Appalachian landmass, Appalachian Mountains (AM), Ouachita Mountains (OM), Hudson Seaway (HS) and Labrador Seaway (LS). Modern North American coastlines and country borders (solid black lines) have been palaeo-rotated onto palaeoDEMs.

Figure 2: Palaeoclimate data from the HadCM3L general circulation model (GCM), which includes mean annual temperature at Earth's surface for the Cenomanian (part **A**) and Turonian (part **B**) North American continent, and mean annual precipitation for the Cenomanian (part **C**) and Turonian (part **D**) North American continent. Solid black lines illustrate (highstand) palaeoshorelines of palaeo-digital elevation models (palaeoDEMs).

Figure 3: Reconstructed location of major drainage systems across the Cenomanian (part **a**) and Turonian (part **b**) North American continent, from calculation of flow accumulation in palaeo-digital elevation models (palaeoDEMs). Flow accumulation is a measure of how many cells flow into each downslope cell. In the figure, flow accumulation ranges from low, 0 cells, to high, 8000 cells (palaeoDEM cells have a resolution of ~11 × 11 km, or 0.1°), and high flow accumulations are therefore predictive of the location of relatively major drainage networks. Solid black lines illustrate (highstand) palaeoshorelines of palaeoDEMs.

Figure 4: Palaeodrainage networks derived for the Cenomanian (part **A**) and Turonian (part **B**) North American continent, which are considered to broadly reflect true palaeodrainage network configurations. Part **A**, inset, illustrates palaeocatchments that are reconstructed from the Cenomanian palaeo-digital elevation model (palaeoDEM) whereas part **B**, inset, illustrates palaeocatchments that are reconstructed

from the Turonian palaeoDEM. Suspended sediment discharges (*Qs*) in palaeocatchments labelled D1, D2, F1 and F2 are compared with published constraints in the Results section. Note that scale bars in the insets are approximate due to use of a conic projection.

Figure 5: Workflow diagram summarising the method to reconstruct suspended sediment discharges (*Qs*) and catchment-averaged erosion rates from palaeo-digital elevation models (palaeoDEMs) and general circulation model (GCM) results using the BQART model (Equation 1).

Figure 6: Cumulative frequencies of catchments relative to their drainage area (part **A**), maximum relief (part **B**), mean annual temperature (part **C**) and mean annual precipitation (part **D**), ordered from smallest to largest, for the Cenomanian, Turonian and modern (ASTER, GTOPO30) North American continent. Catchment geometries and climates are derived from palaeo-digital elevation models (palaeoDEMs) and HadCM3L general circulation model (GCM) data for the Cenomanian and Turonian North American continent, and from the ASTER and GTOPO30 global DEMs (GDEMs) and WorldClim data sets for the modern North American continent.

Figure 7: Univariate and multivariate sensitivity of our approach to unknown uncertainties in palaeogeographic and palaeoclimatic boundary conditions. We show the univariate (parts **A**, **C, E, G**) and multivariate (parts **B**, **D, F, H**) sensitivity of our *Qs* estimates to 10%, 20%, 30%, 40% and 50% uncertainty margins on A, R, and P, and to ±1, ±2, ±3, ±4, ±5 uncertainty margins on T. Solid black lines represent the minimum and maximum *Qs* values predicted in this study when using a range of error margins on boundary conditions for D1, D2, F1 and F2. For univariate sensitivity, solid black lines are presented as error bars, and uncertainty margins increase, left to right, from 10% to 50%/±1 to ±5 for each parameter. For multivariate sensitivity, solid black lines are presented as minimum and maximum curves, and uncertainty margins are depicted on the X axis. Dashed black lines represent the minimum and maximum values of suspended sediment discharge (*Qs*) predicted in published literature for both the Cenomanian Dunvegan Formation, Alberta, Canada (parts **A–D**), and the Turonian Notom delta complex of the Ferron Sandstone, Utah, USA (parts **E–H**).

Figure 8: Spatial distributions of suspended sediment discharges (*Qs*) for the Cenomanian (part **A**) and Turonian (part **B**) North American continent, as well as spatial distributions of catchment-averaged erosion rates for the Cenomanian (part **C**) and Turonian (part **D**) North American continent. *Qs* values are grouped by orders of magnitude whereas catchment-averaged erosion rates are grouped by equal intervals (see colour ramps). *Qs* values and catchment-averaged erosion rates overlay palaeo-digital elevation model (palaeoDEM) hillshades for comparison with palaeotopography.

Figure 9: The cumulative frequency of palaeocatchments relative to their suspended sediment discharges (*Qs*) values (part **A**) and catchment-averaged erosion rates (part **B**), ordered from smallest to largest, for both the Cenomanian and Turonian North American continent.

Figure 10: Latitudinal variation in suspended sediment discharges (*Qs*) and catchment-averaged erosion rates for a north–south transect along the western margin of the Western Interior Seaway (WIS). Latitudinal variation in *Qs* values are depicted for the Cenomanian (part **A**) and Turonian (part **B**), and latitudinal variation in catchment-averaged erosion rates are also depicted for the Cenomanian (part **C**) and Turonian (part **D**). Insets in parts **A** and **B** illustrate highstand palaeoshorelines of the Cenomanian and Turonian North American continent (solid black lines) and the transect location (dashed black line). Uncertainty margins are plotted (bars in parts **A** and **B**, dashed lines in parts **C** and **D**) based on adoption of 10%/±1° uncertainty on all palaeogeographic and palaeoclimatic boundary conditions.

Table 1 – Lyster et al.

	Stage age (Ma)	Stage duration (Myr)	PalaeoDEM reconstruction age (Ma)
Cenomanian	93.9–100.5	6.6	96.6
Turonian	89.8–93.9	4.1	91.4

Table 2 – Lyster et al.

	Number of palaeocatchments reconstructed	Drainage area (km^2)			Maximum relief (m)		
		Minimum–maximum	Median	Mean	Minimum–maximum	Median	Mean
Cenomanian	1623	510–993,000	2,680	10,800	1–4,240	460	1,180
Turonian	1742	510–830,000	2,890	9,290	1–4,310	649	1,240

Table 3 – Lyster et al.

	Mean annual temperature (°C)			Mean annual precipitation (mm/yr)		
	Minimum–maximum	Median	Mean	Minimum–maximum	Median	Mean
Cenomanian	−6.3–30.3	9.7	11.0	317–3,090	800	969
Turonian	−10.2–29.8	7.7	8.7	260–2,510	852	1,050

Figure 1 – Lyster et al.

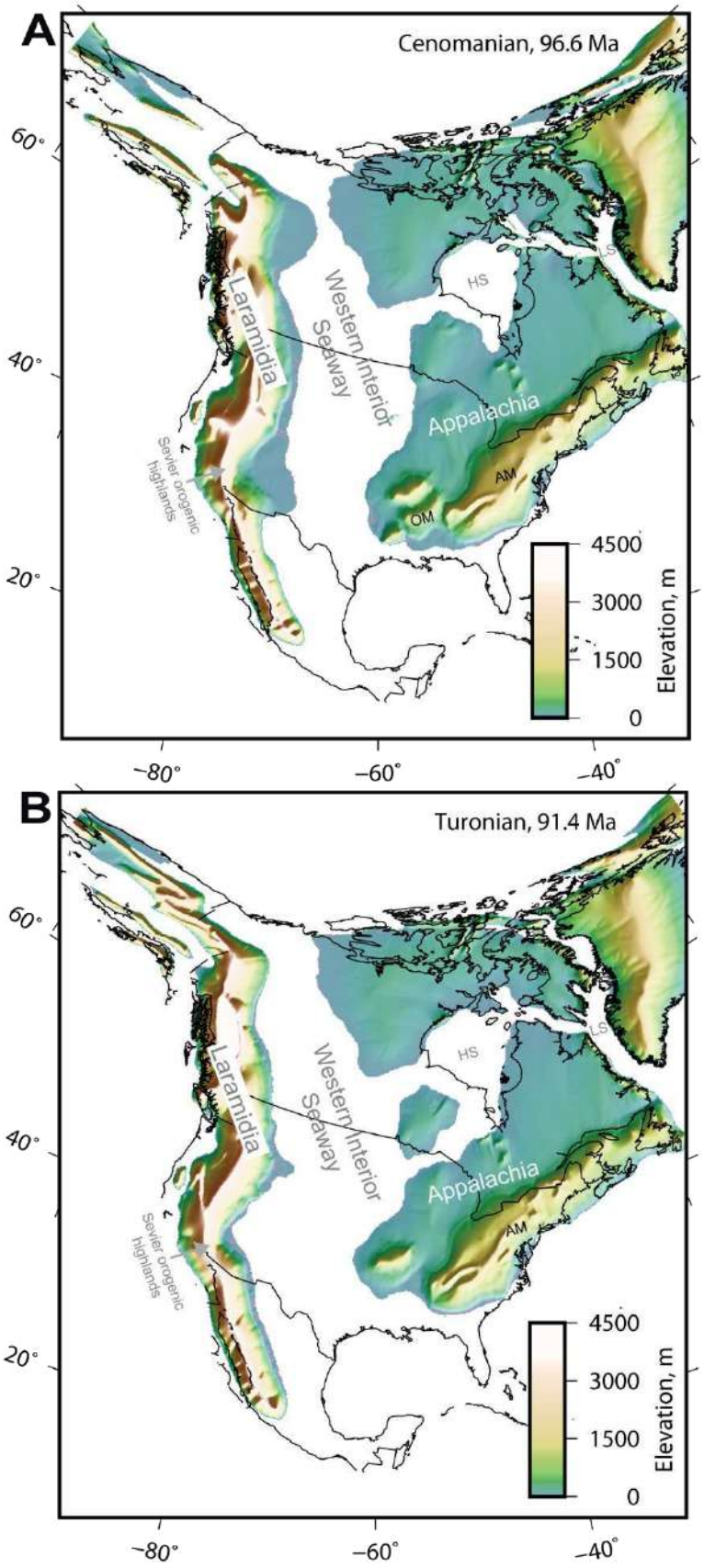

Figure 2 – Lyster et al.

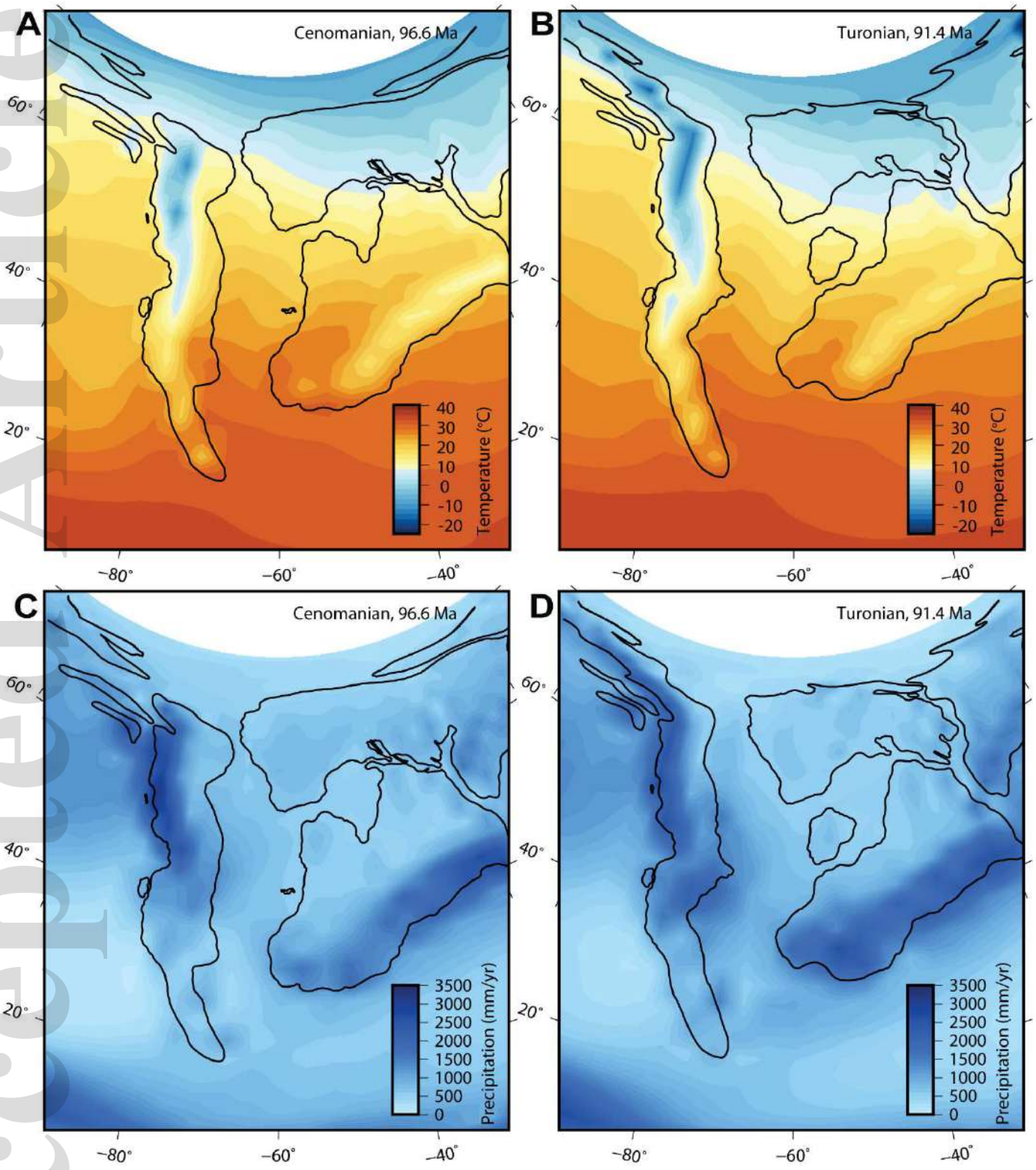

Figure 3 – Lyster et al.

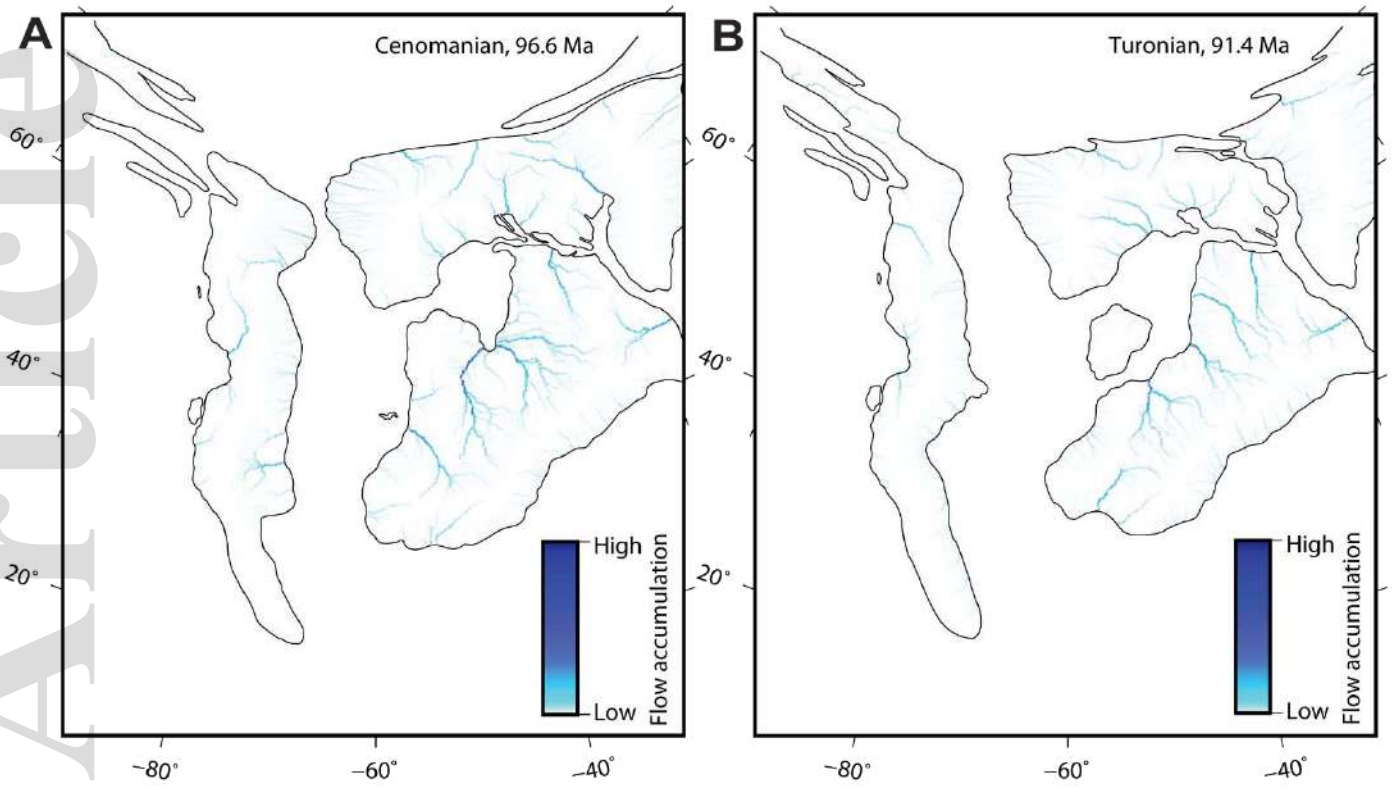

Figure 4 – Lyster et al.

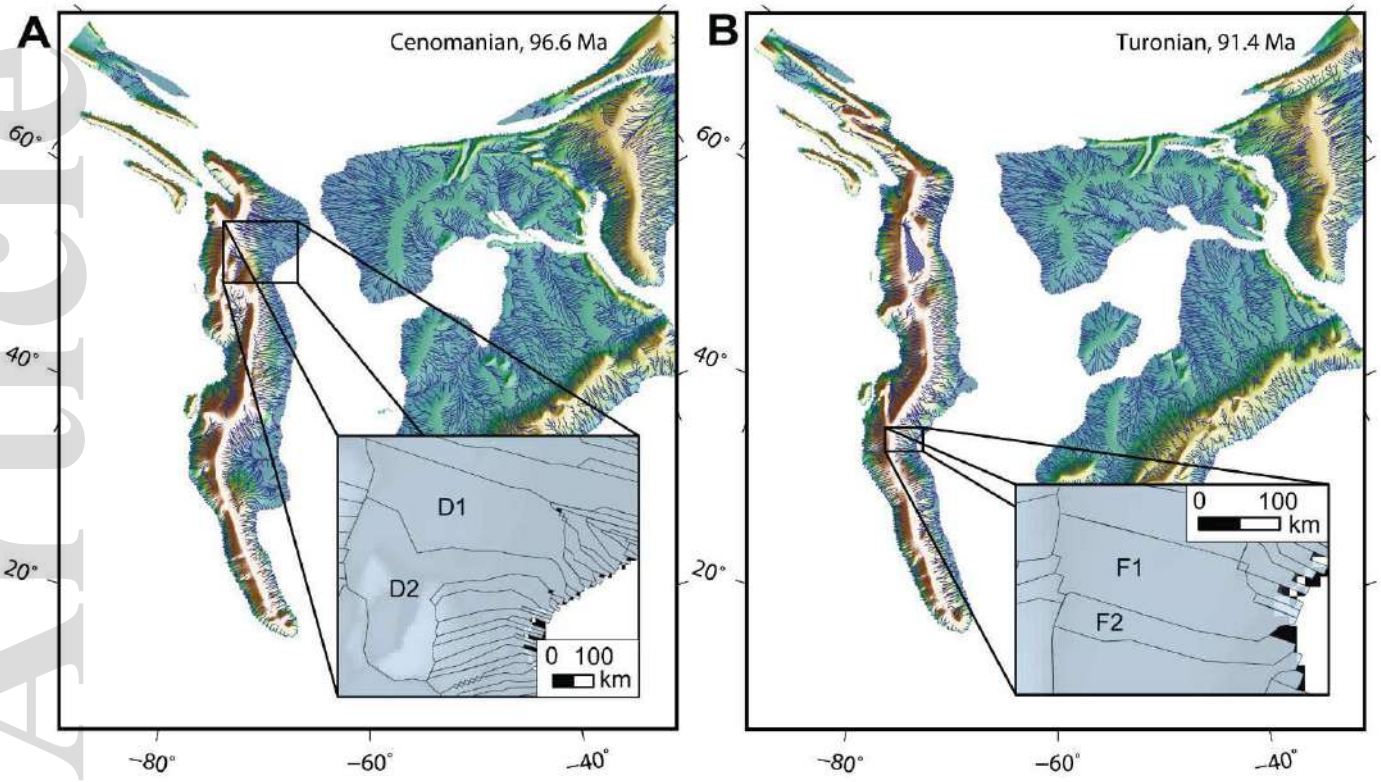

Figure 5 – Lyster et al.

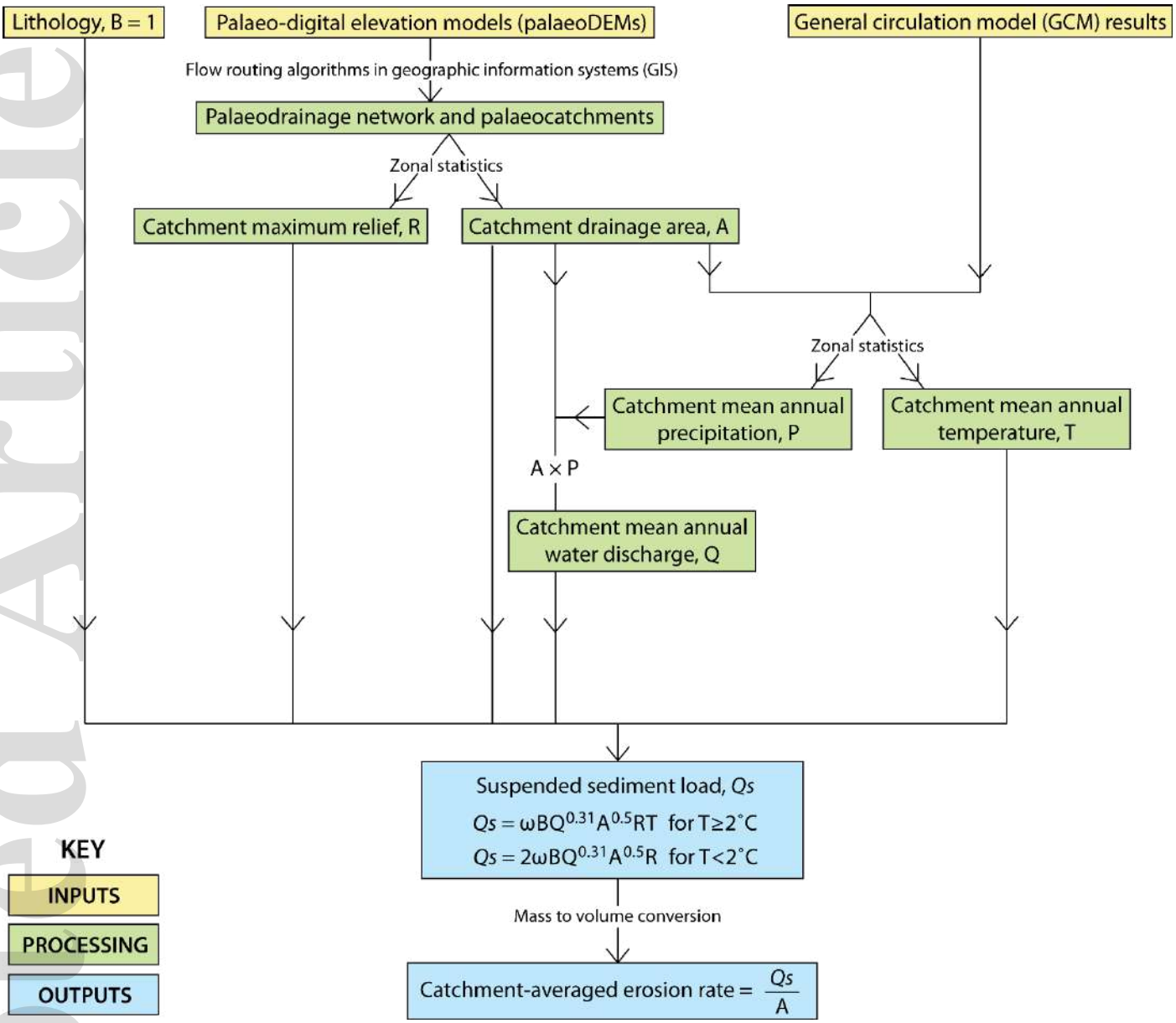

Figure 6 – Lyster et al.

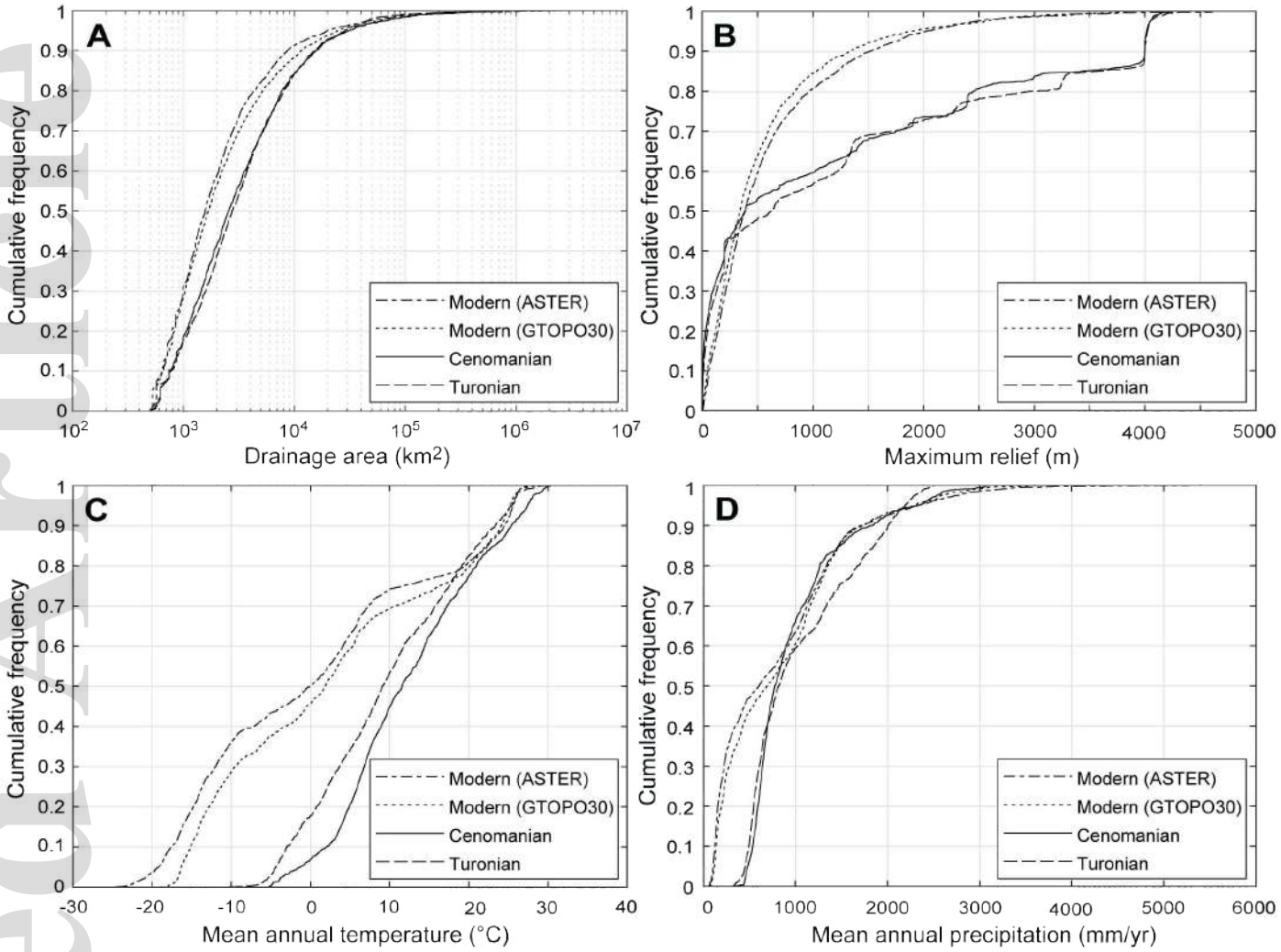

Figure 7 – Lyster et al.

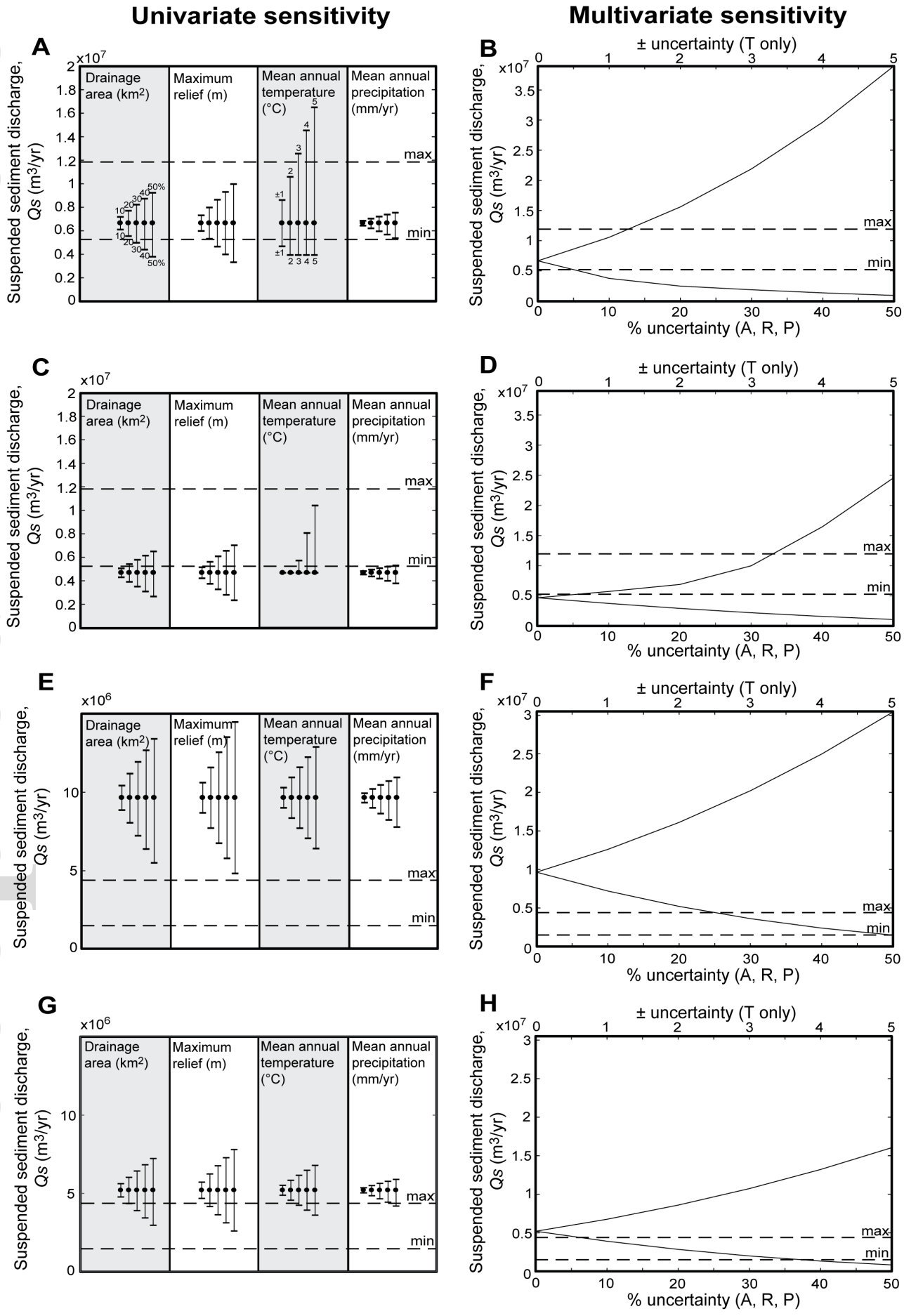

Figure 8 – Lyster et al.

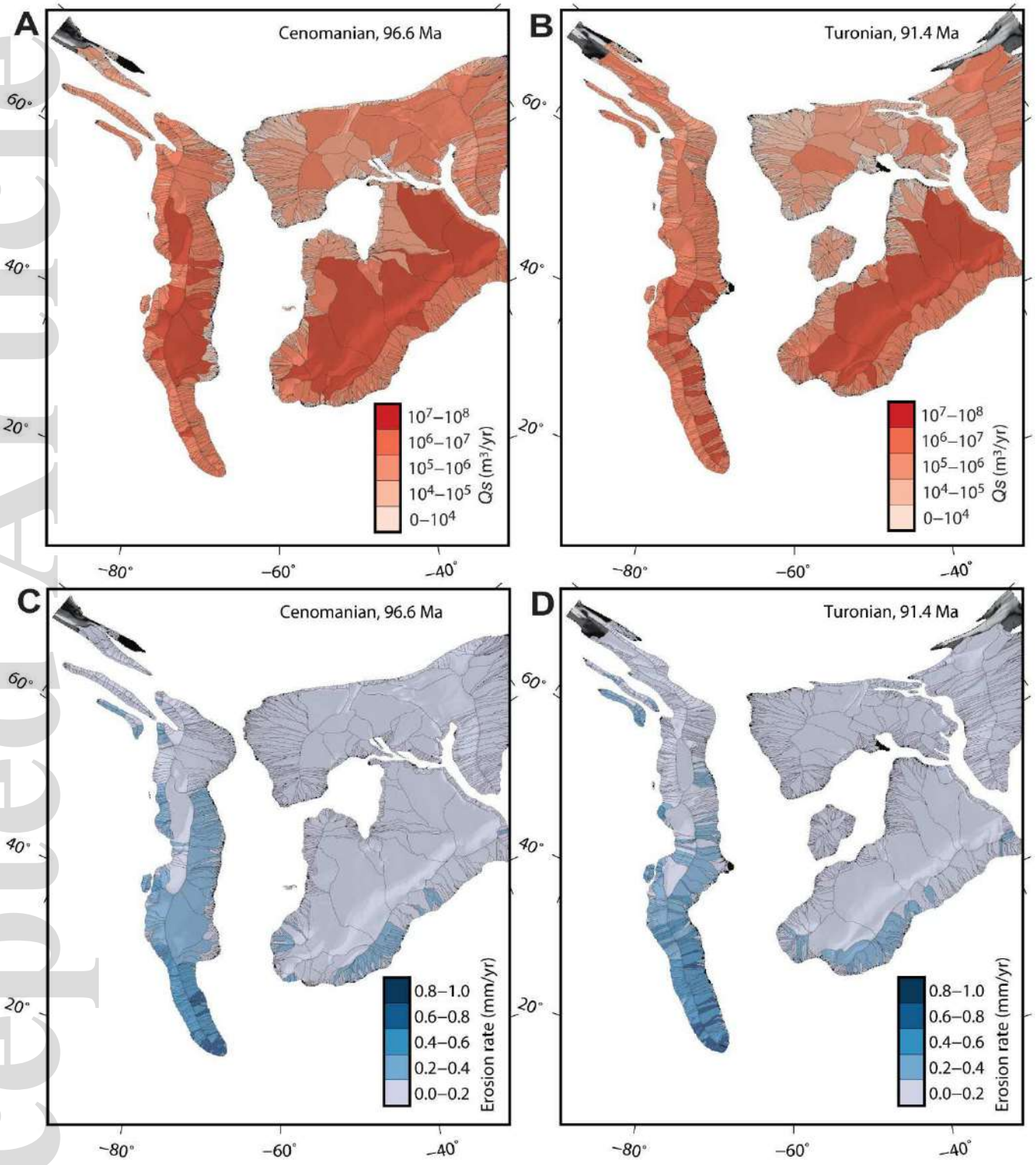

Figure 9 – Lyster et al.

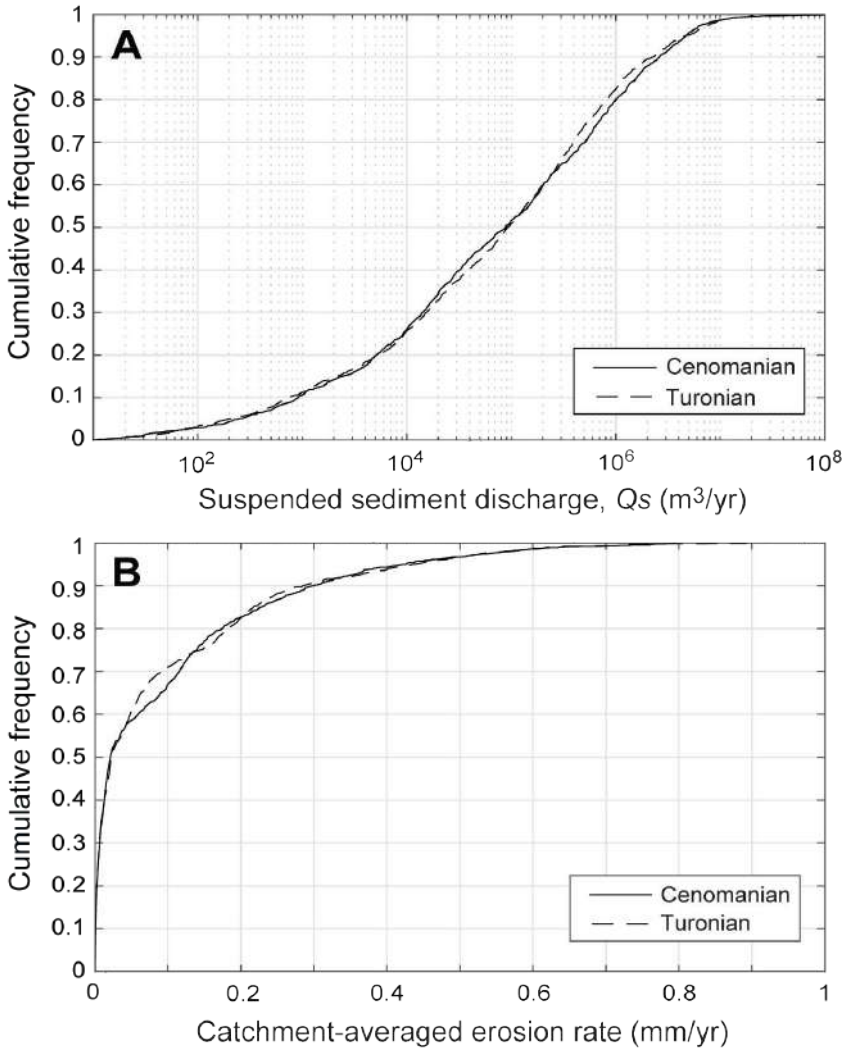

Figure 10 – Lyster et al.